Surface & Coatings Technology 485 (2024) 130901

Contents lists available at ScienceDirect

Surface & Coatings Technology

journal homepage: www.elsevier.com/locate/surfcoat

Full length article

Surface engineering of aerospace aluminium alloys: Understanding alloying effects on chemical pre-treatment and sol-gel coating adhesion

J.P.B. van Dam [a,1], U. Tiringer [a,b,1], S.T. Abrahami [a], I. Milošev [b], H. Terryn [c], J. Kovač [d], J.M. C. Mol [a,*]

[a] Delft University of Technology, Department of Materials Science and Engineering, Mekelweg 2, 2628 CD Delft, the Netherlands
[b] Jožef Stefan Institute, Department of Physical and Organic Chemistry, Jamova c. 39, SI-1000 Ljubljana, Slovenia
[c] Department of Materials and Chemistry, Research Group Electrochemical and Surface Engineering (SURF), Vrije Universiteit Brussel, Pleinlaan 2, B-1050 Brussels, Belgium
[d] Jožef Stefan Institute, Department of Surface Engineering, Jamova c. 39, SI-1000 Ljubljana, Slovenia

ARTICLE INFO

Keywords:
Sol-gel
Surface pre-treatment
Aluminium
Aluminium alloys
Surface chemistry
Surface morphology
Wettability
Adhesion
Adhesive

ABSTRACT

The sol–gel process is a chemical surface preparation method based on hydrolysis and polycondensation reactions for enhanced adhesion for metallic substrates in adhesive bonding and coating applications. This paper describes an investigation into the effect of the microstructural complexity of two commonly used aerospace aluminium alloys (AAs) 2024-T3 and 7075-T6, on the response to different surface pre-treatments before deposition of the sol-gel coating and subsequent adhesive bonding.

Different surface pre-treatments, including two abrasive treatments and three chemical surface pre-treatments were used, and their effect on surface chemistry, wettability and roughness was assessed. Surfaces were characterized by scanning electron microscopy, X-ray photoelectron spectroscopy, profilometry and static contact angles. A hybrid silane sol-gel film was deposited on the differently pre-treated aluminium alloys, an epoxy adhesive was applied and the adhesion properties were evaluated using pull-off testing. The role of the altered physicochemical properties of the pre-treated surfaces was related to the adhesion strength of the sol–gel reinforced epoxy/aluminium interfaces.

The microstructural complexity of the aerospace alloys caused non-uniform responses to the pre-treatments, proving the importance of compatibility between material and treatment conditions. Statistical analysis revealed that, despite that overall higher adhesion values were obtained on rougher surfaces, only a strong correlation exists between the surface hydroxyl fraction and adhesion strength. The relation of roughness and water contact angle to interfacial adhesion was found to be non-significant.

The findings of this study underscore the critical role of surface pre-treatments and their impact on adhesion strength in aerospace aluminium alloys, providing valuable insights for the effective utilization of sol-gel coatings in adhesive bonding and coating processes.

1. Introduction

Adhesive bonding of aluminium alloys (AAs) has become increasingly important in a multitude of industries, such as the aircraft, automotive and maritime industries [1,2]. The use of adhesive bonding, either by itself or in conjunction with other joining techniques, provides significant advantages over traditional joining techniques, such as lower weight, cost and improved mechanical performance [3]. Two commonly used aluminium alloys for aircraft applications are AA2024-T3 and AA7075-T6, particularly because of their high strength-to-weight ratio [4,5]. Both alloys contain various intermetallic particles (IMPs) constituted from Al, Cu, Mg, Zn, Si, etc. [6–8], which all may induce various surface reactions in response to different chemical surface pre-treatments. The alloying element thereby have a significant influence on the physicochemical surface properties of the individual treated aluminium alloys [9–11]. As a result, the alloy composition and its IMPs have a major influence on both the inherent corrosion behaviour or susceptibility [12–19] as well as on the interfacial bonding strength with

* Corresponding author.
E-mail address: J.M.C.Mol@tudelft.nl (J.M.C. Mol).
[1] These authors have equally contributed to the manuscript.

https://doi.org/10.1016/j.surfcoat.2024.130901
Received 29 February 2024; Received in revised form 7 May 2024; Accepted 8 May 2024
Available online 9 May 2024

subsequent overlayers [20–23]. However, it is widely acknowledged that aluminium alloys AA2024-T3 and AA7075-T6 are inherently prone to corrosion, despite the application of pre-treatments and organic overlayers [24–27]. Consequently, a major concern is the initial dry adhesion as well as the potential deterioration in mechanical performance of adhesive joints that incorporate these aluminium substrates due to wet or corrosive de-bonding when subjected to harsh service environments [28,29].

The pre-treatment of the aluminium substrate is essential to ensure life-long integrity of the adhesive bond in practical applications. Aluminium alloys are therefore commonly subjected to multistep surface conditioning pre-treatments [30–33]. The main goal of surface pre-treatments is to modify surface oxide chemistry, remove contaminants, enhance surface roughness, wettability and adhesion, and improve the corrosion resistance of the aluminium (alloys) [34]. The exact surface pre-treatment procedure varies strongly, depending on factors such as alloy type, desired performance, application method, environmental considerations, and compliance with standards and regulations. For processing of high strength aluminium alloys used in the aerospace industry, typical surface conditioning treatments to improve the surface properties of aluminium substrates begin with alkaline cleaning to remove surface aluminium oxides as well as saponify oily residues [35]. Cleaning is typically followed by acidic deoxidizing or de-smutting, commonly employing nitric acid, to remove insoluble oxides formed during the alkaline cleaning process, [36–38]. Each step in the conditioning treatment process induces alterations in the microstructure, morphology, chemistry, and composition of the surface, arising from the procedures [35]. Subsequently to surface conditioning treatments, additional treatment of the surface, such as anodizing [39–41] and chemical conversion coatings [42,43], can be used to further enhance surface properties, improve corrosion resistance and attain higher adhesion strengths.

The drawback of these processes arises from the use of strong acids, bases, and other hazardous substances, such as chromates. Sol-gel coatings present a promising alternative. They offer environmentally friendly production methods, are non-toxic, and exhibit readily tuneable properties through precursor mixture adjustments [44].

Organic-inorganic hybrid (OIH) sol-gel materials bridge the organic and inorganic domains, allowing for the fabrication of nanoscale composite materials with customizable physical and chemical properties [45]. The presence of organic functional groups enhances flexibility, reducing susceptibility to cracking and improving barrier properties, while the inorganic constituents enhance mechanical strength and promote adhesion to metal substrates [46–48].

Numerous studies have highlighted the ability of the silicon alkoxide-based inorganic precursors of OIH sol-gels to form covalent bonds with aluminium substrates (Si-O-Al) through surface hydroxyl groups [49,50]. This bonding ability creates an interfacial region characterized by supreme adhesion and enhanced long-term stability between the aluminium substrate and subsequent overlayers [51–54]. Recent work on silicon alkoxide-based OIH sol-gel films has demonstrated their potential as promising treatment for both enhanced adhesion performance [55,56] and improved corrosion protection on AA2024-T3 and AA7075-T6 [57–60]. In this case, the inorganic part of the hybrid sol-gel coating, the tetraethyl orthosilicate (TEOS), reacts with the aluminium substrate to produce covalent bonds, while the organic part, 3-glycidoxypropyltrimethoxysilane (GPTMS), interacts with the polymer overcoat via the epoxy ring [61–63].

While considerable research attention has been directed towards OIH sol-gels for anti-corrosion protection, often in conjunction with corrosion protective topcoats [64–67], there is a lack of literature addressing their performance in adhesive bonding despite their enormous potential in this field. Similarly, while numerous studies have investigated both the influence of sol-gel application parameters and surface pre-treatments on the adhesion performance of sol-gel coatings to AA2024 and AA7075 alloys [55,64,68,69], solely the role of the physicochemical surface properties of the aluminium alloys on the adhesion promoting properties of these sol-gels has not been a topic of investigation yet.

In our earlier work, the effect of several surface treatments on the chemical and morphological surface properties of commercially pure aluminium (AA1050) and subsequent adhesion of sol-gel films was studied [70]. It was demonstrated that the application of the hybrid sol-gel film induced a significant increase in adhesion strength. But more importantly, a strong correlation between surface chemistry, in particular the hydroxyl fraction, and interfacial adhesion of the sol-gel was found. Expanding upon the preceding section regarding the impact of alloying elements on the physicochemical surface properties of treated alloys, it is crucial to investigate the alloys' response to different pre-treatments and the direct correlation with subsequent bonding interactions. Such investigation is pivotal to understanding how these treatments can effectively be utilized in surface engineering of aerospace aluminium alloys to enhance adhesive bonding.

In the current work, our methodology on commercially pure aluminium is extended to AA2024-T3 and AA7075-T6 in order to understand how surface chemistry and morphology are influenced by the presence of alloying elements and how the obtained surfaces directly correlate to sol-gel adhesion. Hence, the effect of alkaline cleaning/etching (KOH), acidic deoxidising (HNO_3), and thermochemical (DI boiling water) pre-treatments on the adhesion of subsequent silane-based hybrid sol-gel layers on AA2024-T3 and AA7075-T6 was studied. The first two treatments (alkaline and acid) are chosen for their widespread use in industrial cleaning procedures. The third treatment (thermochemical) is well-documented in literature as an effective method for inducing the formation of a highly hydrated and porous surface, primarily consisting of pseudo-boehmite (AlO(OH)·nH2O) [71]. Given that the adhesion of the silicon alkoxide precursors is significantly influenced by the metal surface condition and the presence of hydroxides and hydrated species, the formation of various oxides plays a crucial role in the interaction between metal oxide and silanols.

The surfaces of the differently pre-treated surfaces were characterized by scanning electron microscopy (SEM-EDS), X-ray photoelectron spectroscopy (XPS), surface profilometry and static contact angles. A hybrid sol-gel coating with incorporated cerium nitrate, which has proven to have additional corrosion protective properties [72–74], was deposited on differently pre-treated aluminium alloys, and its effect on adhesion to the subsequently applied hybrid sol-gel coating was assessed using pull-off testing. Evaluation of the significance of the individual contributions of surface chemistry versus morphology on surface wettability and adhesion was performed through a bivariate Pearson correlation.

The present paper is a step towards understanding the true relationship between the chemical and morphological changes induced on the surface by different conditioning treatments, and the adhesive properties of OIH sol-gel coatings on AA2024-T3 and AA7075-T6 alloys.

2. Experimental

2.1. Schematic sample configuration

The studied sample configuration is presented in Fig. 1 and consists of a base substrate and three distinct layers. The base substrate is aluminium alloy AA2024-T3 or AA7075-T6 (a), which is pre-treated by HNO_3, KOH or boiling DI water (b). The pre-treatment of the base substrate is followed by GPTMS, TEOS, SiO_2, $Ce(NO_3)_3$-based hybrid sol-gel coating deposition (c) and finally by 2k epoxy – Araldite polymeric adhesive application (d). Application procedures for each layer are described in a separate section.

2.2. Substrate surface preparation

Substrates used in the present work are aluminium alloys AA2024-T3

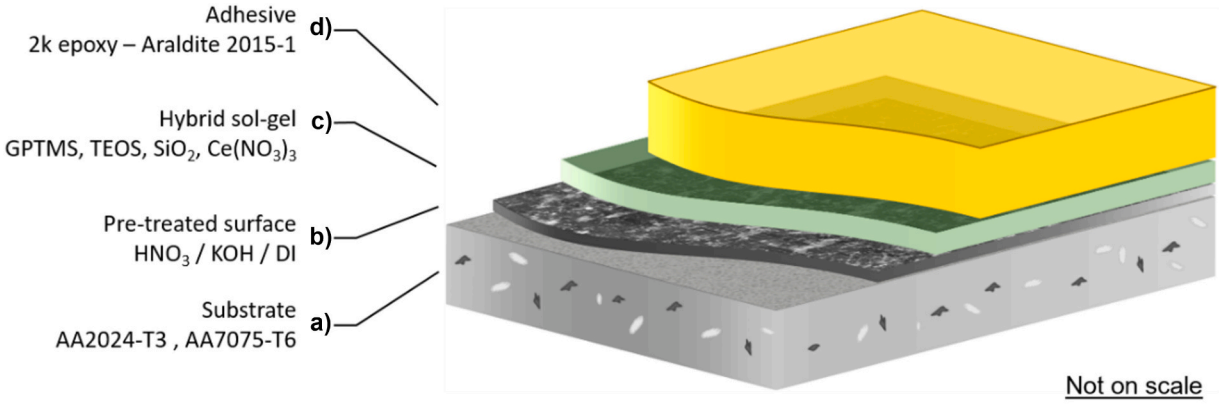

Fig. 1. Schematic sample configuration studied in this work: (a) the base substrate, (b) the pre-treatment layer, (c) the sol-gel coating and (d) the polymeric adhesive.

and AA7075-T6, supplied by Kaiser Aluminium. Their nominal composition is presented in Table 1.

Firstly, AA2024-T3 and AA7075-T6 samples were mechanically abraded with SiC paper, one series up to 4000 grit and another to 800 grit. After grinding, samples were ultrasonically cleaned in ethanol for 10 min and dried under a flow of air.

As-prepared samples are labelled "4000grit_2024 / _7075" or "800grit_2024 / _7075" and represent abraded reference samples without subsequent surface pre-treatment. The reference samples of the AA2024-T3 and AA7075-T6 alloys were subsequently used as precursors for several pre-treatment processes (acid, alkaline and thermochemical). Immersion for 3 min at 57 °C in a 3 vol% KOH solution (pH 10.8) was used as a non-commercial alkaline cleaning treatment. Deoxidation or de-smutting of the surface through acid treatment, consisted of 30 s immersion in a 30 vol% aqueous HNO_3 solution (pH 0.1). The thermochemical treatment was performed by 15 s immersion in boiling deionized water (pH = 7.2). After each treatment, samples were immersed and rinsed with deionized water and dried under a flow of air.

2.3. Sol-gel synthesis and deposition

Silane-based hybrid sol-gel coatings used in the present work were prepared by mixing tetraethyl orthosilicate (TEOS, Aldrich, 99 %), 3-glycidoxypropyltrimethoxysilane (GPTMS, ABCR, 98 %), colloidal silica SiO_2 (Ludox-4S, Aldrich, aqueous suspension 40 wt%) and cerium nitrate ($Ce(NO_3)_3.6\ H_2O$, Aldrich, 98 %) [72–74]. After 30 min of magnetic agitation, 0.6 mL of concentrated HNO_3 (VWR, 65 % aqueous solution) was added as a catalyst for polycondensation. After 10 min of magnetic agitation, absolute ethanol (EtOH, Panreac, 99.8 %) was added as a solvent to obtain a molar ratio of the sol of TEOS/GPTMS/SiO_2/Ce = 0.5/0.5/0.54/0.03 and a molar ratio of EtOH/(TEOS+GPTMS) = 3.8/1. The obtained sol is denoted as GTS-Ce. GTS-Ce sol was applied on aluminium samples through dip-coating, with an immersion and emersion rate of 30 cm/min and a residence time of 1 s. Samples were heat-treated for 1 h at 120 °C to complete the polymerization and bonding between the sol and the substrate. The obtained sol-gel coating thickness is 7.0 ± 0.7 um. For further details on the hybrid sol-gel, the synthesis process or deposition procedure, readers are directed to our earlier works [72–74].

2.4. SEM-EDS

General observations about the morphology and composition of differently pre-treated samples were obtained by scanning electron microscopy equipped with electron dispersive spectroscopy (SEM-EDS) using a backscattered electron detector attached to the EDS system. SEM analysis was performed on a JEOL IT100 Scanning Electron Microscope (SEM) coupled with an EDS analyser at an acceleration voltage of 10 kV. Data were processed with the corresponding InTouchScope™ software. For all samples, EDS analysis of a relatively large area (65 μm × 50 μm) was chosen to record the general changes in elemental surface composition upon pre-treatment. Surface analysis through SEM-EDS was performed within a few minutes after preparation of the differently pre-treated surfaces to avoid superficial changes e.g. excessive oxidation or adventitious contamination.

2.5. XPS

X-ray photoelectron spectroscopy (XPS) was used for surface compositional and hydroxyl fraction determination of differently pre-treated AA2024-T3 and AA7075-T6 samples. Since the relative surface hydroxyl (OH-) fraction is mostly a result of chemical modification and not of surface roughness [70], the XPS was measured only for finely abraded samples (4000 grit).

PHI-TFA XPS spectrometer (Physical Electronic Inc.), equipped with an X-ray Al-monochromatic source, was used for analysis. The vacuum during XPS analysis was 10^{-9} mbar. The analysed depth was 3– 5 nm, and the area was 0.4 mm in diameter. Multiplex scans of the peaks were recorded using a pass energy of 29 eV with a step-size 0.1 eV. A take-off angle was 45° with respect to the sample surface. Spectra were interpreted using Multipak v8.0 (Physical Electronics Inc.) software. Surface analysis through XPS was performed within a few minutes after preparation of the differently pre-treated surfaces to avoid superficial changes e.g. excessive oxidation or adventitious contamination.

The elemental composition at the near-surface region was determined from the XPS survey spectra. For each sample, three high-energy XPS spectra of elements detected by survey analysis, were recorded at different regions. The relative amounts of hydroxyl fractions were calculated from fitted high-energy resolution spectra of O 1 s and C 1 s

Table 1
Nominal composition (wt%) of AA2024-T3 and AA7075-T6.

Substrate	Nominal composition (wt%)								
	Al	Cu	Mg	Fe	Si	Mn	Zn	Ti	Cr
AA2024-T3	90.7–94.7	3.8–4.9	1.2–1.8	0.5	0.5	0.3–0.9	0.3	0.2	0.1
AA7075-T6	87.1–91.4	1.2–2.0	2.1–2.9	0.5	0.4	0.3	5.1–6.1	0.2–0.3	–

photoelectron peaks. C 1 s was fitted to consider the atmospheric contamination, which is always obtainable and is shown as C 1 s peak. O 1 s is deconvoluted into O^{2-}, OH^- and adsorbed H_2O, while C 1 s into C–C/C–H, CO and COOX components. Fig. 2 presents deconvoluted spectra of O 1 s (a) and C 1 s (b) of bare AA2024-T3 as an example. The remaining deconvoluted spectra are not shown but were obtained in an identical way. Limitation parameters applied for curve fitting the O 1 s and C 1 s high-resolution spectra are presented in Table 2.

The model used for OH-fraction calculations was developed by McCafferty and Wightman, which considers the contribution of atmospheric contamination to the relative amount of OH-fractions [75]. This means that the contributions of CO and COO^- are taken into account in O 1 s peak (Fig. 2).

The fitted intensity areas were used to find a solution for the amount of O^{2-}, OH^- and H_2O, while taking into account the intensity originating from oxygen species, which are provided by the intensities of the fitted C—O and O=C–O sub-peak areas in C 1 s (Fig. 2). The relative amount of OH-fraction of differently pre-treated AA2024-T3 and AA7075-T6 were determined through Eq. (1).

$$OH^- (\%) = \frac{c_{OH^-}}{c_{OH^-} + c_{O^{2-}} + c_{H_2O}} * 100 \quad (1)$$

2.6. Surface topography

The surface topography of differently pre-treated AA2024-T3 and AA7075-T6 was evaluated using a Bruker DektakXT profilometer, with a lateral resolution of 1 μm and a vertical resolution of 5 nm. The area of the measured spots was 1 × 2 mm. The obtained data were processed with TalyMap Gold software v6.2, in accordance with ISO 25178, allowing for 3-D surface topography construction and calculation of roughness parameters: arithmetic surface roughness (S_a), skewness (S_{sk}), kurtosis (S_{ku}), maximum height (S_z) and root mean square height (S_q). Topographical measurements were performed threefold and average values with standard deviations were reported.

2.7. Surface contact angles

The wettability of the differently pre-treated surfaces was evaluated by measuring static water contact angles using a Kruss DSA 100 Easy Drop Standard System. Static water contact angles were measured in three areas to obtain average static contact angles and standard deviations. Analysed surfaces were considered hydrophilic and the wettability of the solid as high, if the static water contact angle (CA) was below 90° and considered hydrophobic and with poor wettability if the static water contact angle was above 90° [76].

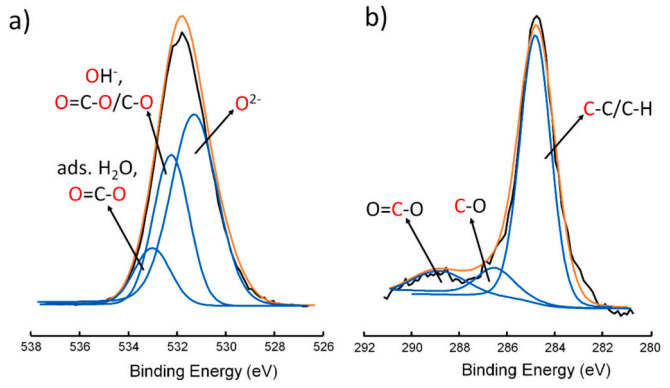

Fig. 2. Deconvoluted XPS O 1 s peaks (a) and C 1 s peaks (b) of bare AA2024-T3 used for O 1 s and C 1 s peak fitting. The blue curves represent sub-peaks, the black curves the measured curves and the orange curve represent fitted values of measured curves.

Table 2
Limitation parameters applied for curve fitting of O 1 s and C 1 s Multiplex XPS peaks, where FWHM is defined as full width at the half maximum.

O 1 s			C 1 s		
Component	FWHM (eV)	Position lock (eV)	Component	FWHM (eV)	Position lock (eV)
O^{2-}	1.80–1.84	0	*CC/CH*	1.6	0
OH^-	1.68–1.72	1.1–1.2	*CO*	2.0	1.5
H_2O	2.07–2.09	2.43	*COOX*	1.4–2.0	3.8–4.3

2.8. Adhesion

The adhesion between differently pre-treated AA2024-T3 and AA7075-T6 and subsequently applied sol-gel films was measured through pull-off adhesion testing. Pull-off testing was performed using an Elcometer® 106 Pull-Off Adhesion tester, according to ASTM D4541–17. Dollies of 20 mm diameter were attached to the samples using a 2k epoxy-based adhesive. All substrates were bonded within a few minutes after surface pre-treatment or sol-gel application.

In the present work, a commercial two-part epoxy system, Araldite® 2015–1, supplied by Huntsman Advanced Materials (Switzerland) GmbH, was used. Araldite® 2015–1 is a structural DGEBA-based epoxy resin adhesive with an amine curing agent. The two parts were mixed in a 1:1 ratio by using an adhesive application gun equipped with a mixing nozzle. The bondline thickness was controlled at 300 μm using glass beads supplied by Sigma Aldrich. The epoxy was cured at room temperature for 24 h, according to supplier application instructions.

Dollies were pulled off at a pull rate of 0.20 MPa/s. For each condition, three samples for pull-off testing were prepared and tested in order to check the reproducibility and to calculate the average adhesion failure strengths (pull-off strengths) and their standard deviations. After pull-off testing, digital images of fracture surfaces were evaluated to assess the failure mode (A: adhesive, C: cohesive or M: mixed).

2.9. Statistical analysis

In order to evaluate the effect of different pre-treatments and associated OH– fraction, arithmetic average roughness (Sa), static water contact angle (CA) and adhesion, the obtained values were compared to a baseline scenario – bare (before any pre-treatment and without sol-gel coating application). The effect of the different treatments was expressed as the relative increase (%) of the individual variables, calculated by Eq. (2):

$$\text{Relative increase } (\%)_{i,j} = \frac{x_{i,j} - x_{\text{bare,j}}}{x_{\text{bare,j}}} \quad (2)$$

where i represents the type of the pre-treatment, j = OH-fraction/roughness S_a / wettability CA / obtained adhesion, and x represents the obtained value of j after each i. Relative increases were calculated for both finely-ground (4000 grit) and coarsely-ground (800 grit) specimens. Individual values and calculated relative increases are presented in the Supplementary information, Table S 6.

In order to compare the contribution of OH-fraction on the adhesion versus the contribution of S_a on the adhesion, the relative increases of both S_a and OH-fraction versus the relative increase in adhesion are used.

In order to determine correlations between OH-fraction, S_a, CA and adhesion, a Pearson's correlation analysis (r) Eq. (3) and p-value significance Eq. (4) was used.

$$r_{xy} = \frac{\sum_{i=1}^{n}(x_i - \bar{x})(y - \bar{y})}{\sqrt{\sum_{i=1}^{n}((x_i - \bar{x}))^2 \sum_{i=1}^{n}(y_i - \bar{y})^2}} \quad (3)$$

where n represents the sample size or the number of paired data points, x_i and y_i denote the individual values of the corresponding pairwise parameters being compared (OH-fraction, Sa, CA and adhesion).

$$p-\text{value} = r_{xy}\sqrt{\frac{n-2}{1-r^2}} \quad (4)$$

A strong pairwise correlation is considered present if $r_{xy} \geq 0.7$ and $p\text{-}value < 0.01$ [77,78].

3. Results and discussion

3.1. SEM-EDS

General observations regarding the surface morphology and chemical elemental distribution over the differently pre-treated AA2024-T3 and AA7075-T6 substrate surfaces were obtained through SEM-EDS analysis. However, it should be noted that EDS analysis was used to assess the overall surface chemical composition through area scans. Therefore, local chemical concentration variations, such as within the IMPs, can differ significantly from the overall chemical composition.

Fig. 3 shows the differently pre-treated AA2024-T3 surfaces. All surfaces feature characteristic parallel grinding marks across the entire surface. However, it can be observed that the individual treatments have had a significant effect on the overall appearance of the individual surfaces. Table 3 provides the elemental composition obtained by EDS analysis of pre-treated AA2024-T3 surfaces. These results show that in addition to changes in overall appearance, the treatments produce significant alterations in the surface chemistry. The bare reference surface of 4000grit_2024 (Fig. 3a) is composed of Al, O, Mg and Cu. The presence of O can be allocated to both the presence of an oxide layer and possible organic contaminants on the surface, while Cu and Mg are the major alloying elements of AA2024-T3 (see Table 1). The surface of AA2024-T3 after HNO_3 pre-treatment is visually similar to the 4000grit_2024 (Fig. 3b). The presence of IMPs at the surface is more prevalent. EDS results compared to 4000grit_2024 show enrichment of Al and Cu after HNO_3 pre-treatment, while concentrations of O and Mg have decreased (Table 3, Region 2). Reduction of both O and Mg concentrations is associated with oxide removal and Mg dissolution due to the deoxidizing properties of the HNO_3, directly resulting in superficial Cu enrichment, which is in accordance with earlier studies [79]. Furthermore, Cu enrichment results from the galvanic coupling between Cu-rich intermetallics and the surrounding Al matrix, inducing preferential and accelerated dissolution of the aluminium alloy matrix during the pre-treatment process [80,81].

The surface after KOH pre-treatment has an entirely different appearance. The surface texture has altered significantly compared to the bare 4000grit_2024 sample (Fig. 3c). Local etching of the surface has induced a level of porosity while the IMPs are present but less prevalent as for the HNO_3-treated surface. The surface texture of the KOH-treated surface is mostly a result of high pH values (10.8) in which some of the Al is dissolved and Cu is passive, causing the dropping out of the IMPs from the surface due to the local dissolution of the Al matrix [32,82,83].

Table 3
Atomic concentrations [at. %] of elements obtained by EDS analysis at various regions on (1) 4000grit_2024, AA2024-T3 pre-treated with (2) HNO_3, (3) KOH and (4) boiling DI water. Regions (1–4) are denoted on SEM images with yellow squares (Fig. 3).

Region	Al [at. %]	O [at. %]	Mg [at. %]	Cu [at. %]
1	85.9	7.5	5.4	1.2
2	91.2	2.1	2.4	4.3
3	75.4	12.1	2.8	10.7
4	83.5	11.4	2.1	3.0

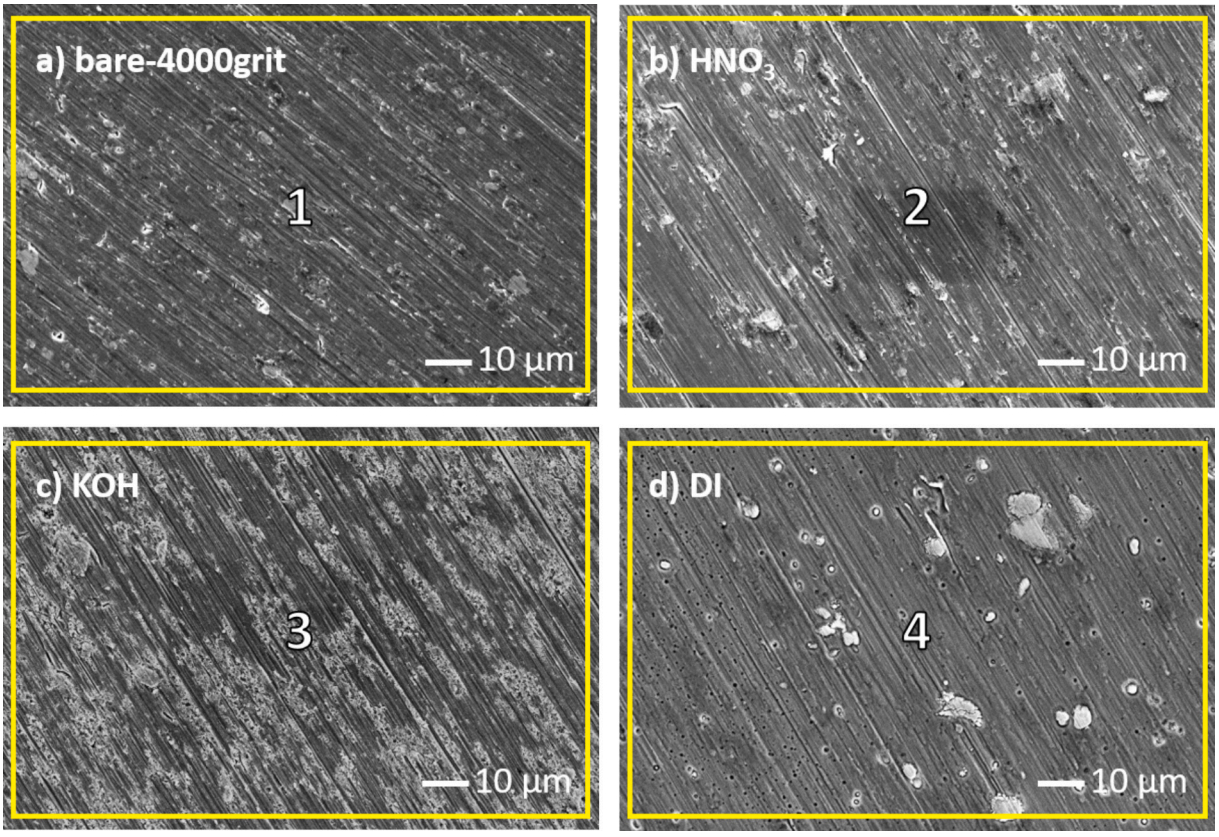

Fig. 3. SEM images of bare 4000grit_2024 (a) and 4000grit_2024 pre-treated with HNO_3 (b), (c) KOH (c) and boiling DI water (d). The yellow squares on the images denote the region where the EDS analysis was carried out and are numbered (1–4) (Table 3). The SEM images were taken in compositional mode.

EDS analysis of AA2024-T3 pre-treated with KOH (Table 3, region 3) shows significantly higher Cu content than the HNO_3-treated specimen, which is in accordance with literature. Rodič et al. found that the alkaline pre-treatment dissolves any superficial Mg-rich constituents, leaving behind a Cu-enriched surface due to the formation of cupric oxide [19]. The dissolution of both the Al matrix and Mg-rich IMPs causes the porous morphology, which is promoted by the galvanic coupling between Cu-rich phases and the Al matrix [13,79,84,85].

Lastly, after the thermochemical pre-treatment with boiling DI water, the Al matrix exhibits a perforated texture, and the IMPs appear clearly on the surface of AA2024-T3 (Fig. 3d). The larger remnants on the surface exhibit a spongy texture and are related to copper deposits, while others to Mg-based IMPs, which is explained more elaborately in our previous work as electrical isolation from the matrix and passivation due to oxide formation [80]. EDS shows similar behaviour of AA2024-T3 pre-treated with boiling DI water as after HNO_3; with a slight increase of Cu and decrease of Mg. Furthermore, a high oxygen concentration was obtained after DI pre-treatment, indicating strong oxide formation.

SEM images of differently pre-treated surfaces AA7075-T6 are shown in (Fig. 4). Once more, the individual pre-treatments have a profound effect on surface appearance and morphology but appear to be less invasive compared to AA2024-T3 (Fig. 3). The surface of 'bare 4000grit_7075' shows a distinctive abrasive pattern, while IMPs are visible (Fig. 4a). The main alloying elements of AA7075-T6 are Zn, Mg and Cu and are found as the main constituents in the EDS analysis (Table 4, Region 1). Once again, although in low quantities, O is found on bare 4000grit_7075, which implies the presence of a native air-formed oxide film at the surface. During the heat treatment of the alloy, magnesium diffuses to the surface which causes a magnesium-rich surface oxide [38]. The surface of AA7075-T6 after subsequent HNO_3 pre-treatment in Fig. 4b clearly shows Cu-rich IMPs. Their presence is more predominant compared to the bare 4000grit_7075 surface. During HNO_3 pre-treatment, anodic Mg- and Zn-rich particles are dissolved as a result of the low pH (0.1), leaving behind a Cu-enriched surface (Table 4, Region 2), which is in accordance with earlier studies [37,42,80]. The increase in O indicates oxide build-up, partially due to aluminium oxide formation and partially due to the Cu-enriched surface leading to subsequent formation of cuprous oxides once exposed.

Table 4
Atomic concentrations of elements obtained by EDS analysis at various regions on bare 4000grit_7075 (region 1), AA7075-T6 pre-treated with HNO_3 (2), KOH (3) and with boiling DI water (4). Regions are denoted on SEM images with yellow squares (Fig. 4).

Region	Al [at. %]	O [at. %]	Mg [at. %]	Zn [at. %]	Cu [at. %]
1	91.7	1.7	3.0	2.7	0.9
2	80.6	9.4	0.3	–	13.7
3	75.1	11.3	4.1	1.8	7.7
4	82.6	9.7	1.0	1.5	5.2

The appearance of the surface and shape of the IMPs after KOH pre-treatment is different compared to the bare and HNO_3-treated surface, see Fig. 4c. Trenching around the IMPs is visible, and the abrasive pattern is less prevalent, both indicating the dissolution of the aluminium matrix.

EDS analysis confirms aluminium dissolution due to high pH (10.8), again resulting in both Cu and Mg enrichment (Table 4, Region 3) [38]. With the oxygen concentration increasing accordingly (Table 4, Region 3), Cu is expected to be mostly present in the form of cuprous oxide Cu_2O. The spongy shape of the Cu IMPs has been observed earlier by Tiringer et al. for AA7075-T6 and explained as electrochemical isolation of IMPs from the matrix and subsequent dissolution of the intermetallic particle [80].

Lastly, after boiling DI water pre-treatment, the surface appearance is similar to the one after HNO_3 pre-treatment (Fig. 4d). Although the responsible mechanism of Cu-enrichment after DI boiling water is not yet fully comprehended, Cu-enrichment is observed nonetheless. However, the concentration increase is less than in the AA7075-T6 surface after the HNO_3 and KOH pre-treatments. Overall, it appears the boiling DI water pre-treatment has a moderate effect on the alteration of the surface appearance and composition and mostly induces the overall strong formation of oxides.

3.2. Surface chemistry analysis

Surface chemistry on differently pre-treated AA2024-T3 and AA7075-T6 samples was characterized by X-ray photoelectron spectroscopy (XPS). XPS survey spectra were acquired before obtaining high-

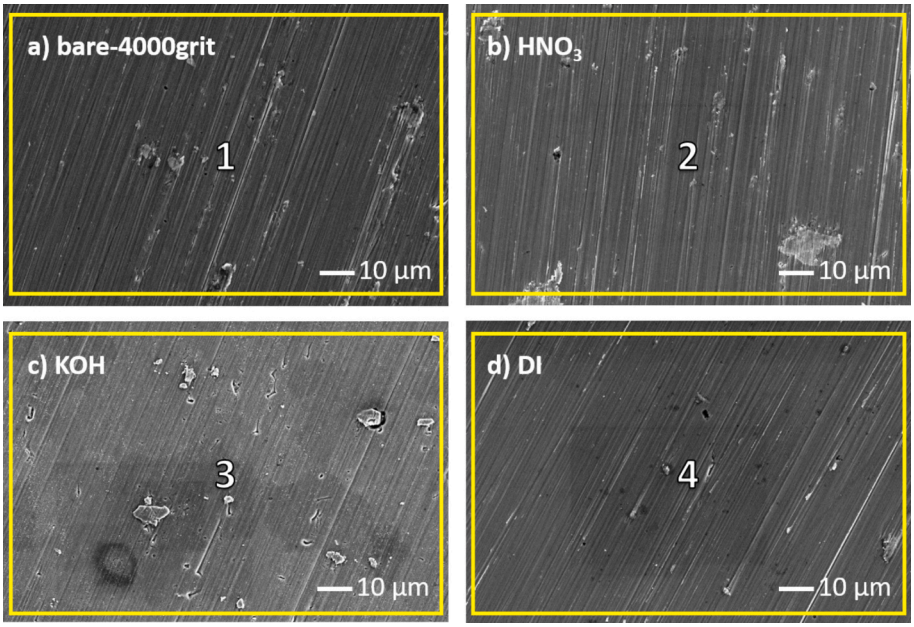

Fig. 4. SEM images of bare 4000grit_7075 (a) and AA7075-T6 pre-treated with HNO_3 (b), KOH (c) and with boiling DI water (d). The yellow squares on the images denote the region where EDS analysis was carried out and are numbered (1–4) (see Table 4).

resolution spectra. Representative XPS survey spectra of the different alloys and treatments are shown in Fig. 5.

A qualitative comparison of the surface chemical composition for the differently pre-treated alloy surfaces, as obtained from the XPS survey spectra, is provided in Table S 4 and Table S 5 of the Supplementary Information. As is to be expected, the major elements at the near-surface region of the untreated substrate are O, C and Al. Carbon can be almost entirely attributed to the presence of ambient organic contaminations. Like carbon, oxygen can be partially attributed to organic contaminants, but a substantial portion can also be ascribed to the aluminium oxide surface layer. Both bare samples show traces of Ca, most probably originating from the cooling water used in the grinding process. The remaining contribution comes from varying concentrations of the alloying elements.

High-resolution spectra (multiplex) of O 1 s and C 1 s were measured and curve-fitted using the method presented in earlier work by Abrahami et. Al [23]. The fitted intensity areas of the photoelectron peaks were subsequently used to derive surface OH-fractions. Results for the differently pre-treated AA2024-T3 and AA7075-T6 surfaces are summarized in Fig. 6. Reported values are average OH-fractions determined from triplicate measurements. The lowest OH-fractions were observed on the bare 4000grit substrates, with 38 % and 39 % on AA2024-T3 and AA7075-T6, respectively. Subsequent pre-treatments in all cases led to an increase of the surface hydroxyl (OH) fractions. In the case of AA2024-T3, HNO_3 (39 %) and KOH (43 %) result in moderate relative increases of +1 and + 5 %. However, boiling DI water pre-treatment (66 %) results in a significant increase of +28 %.

The response in terms of OH-fraction increase on pre-treated AA7075-T6 samples was found to be comparable to the pre-treated AA2024-T3 samples. After HNO_3 (43 %) and KOH (56 %) treatments, moderate to strong relative increases of +4 and + 17 % in OH-fraction were observed. As a result of the DI boiling water treatment (72 %), surface hydroxyl fractions again increased significantly with +33 %.

Overall, the trend of OH-fraction is similar for both substrates, with the lowest hydroxyl fractions observed on bare surfaces and for samples pre-treated with HNO_3. Pre-treatment based on KOH moderately increases the OH-fraction of all substrates, and both high OH-fractions were observed after boiling water pre-treatment, which is in accordance with other studies and has been allocated to pseudoboehmite formation [20,22,23,43].

Interestingly, the trend in relative increase of surface OH-fractions was found to be similar compared to commercially pure Al, as was studied in our previous work, but all concentrations were noticeably higher [70]. This is most likely related to the presence of different alloying elements within the matrix, which can contribute to different species (oxides, hydroxide etc.), which in turn contribute to the OH-fraction.

3.3. Surface roughness

Surface topographical mappings were recorded to assess variations in the surface roughness of the differently-treated surfaces. Fig. 7 shows a topographical map of bare 800grit_7075 displaying the characteristic parallel abrasive marks across the entire surface, as was observed through SEM. From the 3D topographical surface maps, roughness parameters were obtained in accordance with ISO 25178 to express alterations in surface roughness. In order to measure or express the roughness of a surface, numerous roughness parameters can be used, of which the arithmetic mean (S_a), height of the 3D surface profile is the one most commonly used. Nevertheless, merely the S_a is insufficient to evaluate the topography of a surface and describe the surface response to chemical treatment. The skewness parameter (S_{sk}) provides additional topographical information regarding the distribution of the varying heights of the roughness profile and allows for a more intricate description of the roughness profile along with the S_a [86]. A complete listing of all obtained roughness parameters is provided in the Supplementary information, Table S 1 and Table S 2.

The 3D arithmetic surface roughness and skewness values of AA2024-T3 and AA7075-T6 after different pre-treatments are presented in Fig. 8. As stated before, all samples were ground up to 4000grit or 800grit prior to additional chemical surface pre-treatments.

S_a of bare_4000grit AA2024-T3 is 0.07 μm. After the subsequent pre-treatments, HNO_3, KOH and boiling DI water, a slight increase of S_a is observed compared to bare-4000grit, resulting in a relative increase of +2.2, +9.6 and + 19.8 %, respectively.

The measured S_a of bare 4000grit_7075 is 0.06 μm, which is slightly lower compared to the bare4000grit_AA2024-T3. Similar to the response of AA2024-T3, HNO_3, KOH and boiling DI water pre-treatments result in an increase of the arithmetic roughness. However, the relative increases of S_a values are substantially higher for AA7075-T6; +35.9, +43.4 and + 60.1 % respectively. This resembles the non-uniform surface reactions, as observed in the EDS results, causing not only shifts in surface chemical composition but even more so inducing a significant increase in surface roughness.

Also, despite the differences in magnitude, the trend of S_a-response is similar for both substrates: bare 4000grit < HNO_3 < KOH < boiling DI. Hence, it becomes clear that DI boiling water treatment induces the highest increase in the overall S_a. Therefore, it can be concluded that the roughness exhibits a similar trend as the calculated OH- fraction (Fig. 6).

All surfaces exhibit a positive S_{sk}, although varying in magnitudes. This indicates an upward non-normal height distribution, representative for surfaces with more peaks than valleys as a result of the abrasive

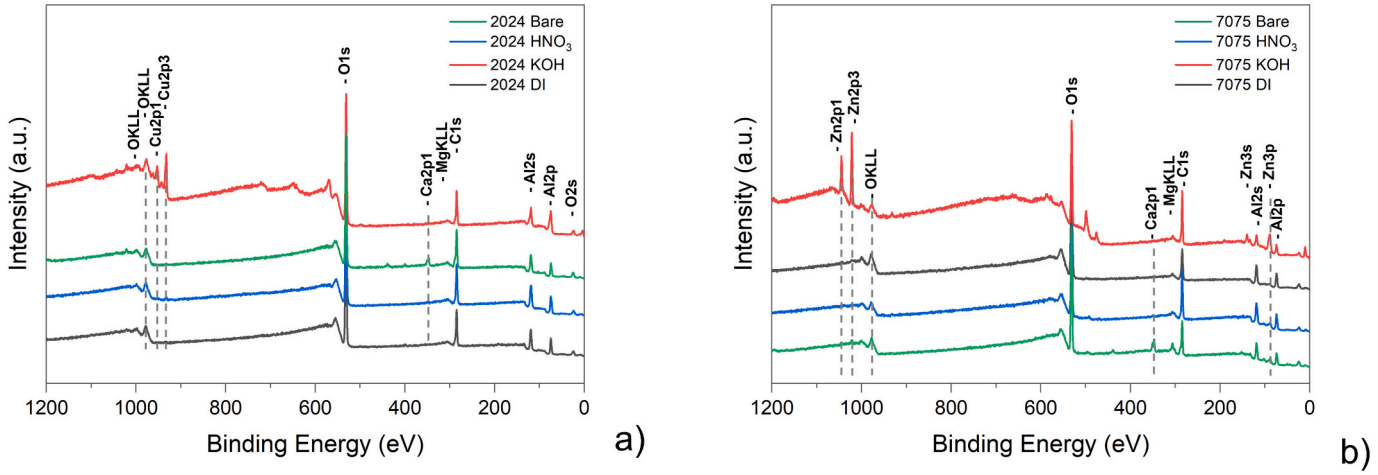

Fig. 5. XPS survey spectra for differently pre-treated surfaces of AA2024-T3 (a) and AA7075-T6 (b).

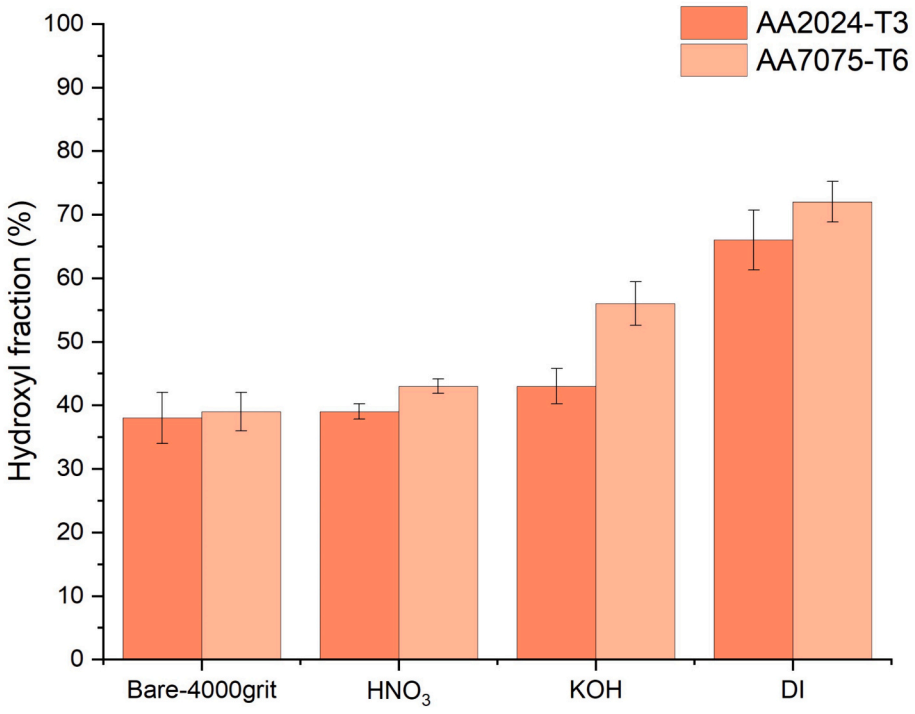

Fig. 6. Hydroxyl fraction for the differently pre-treated 4000grit_AA2024 and 4000grit_AA7075.

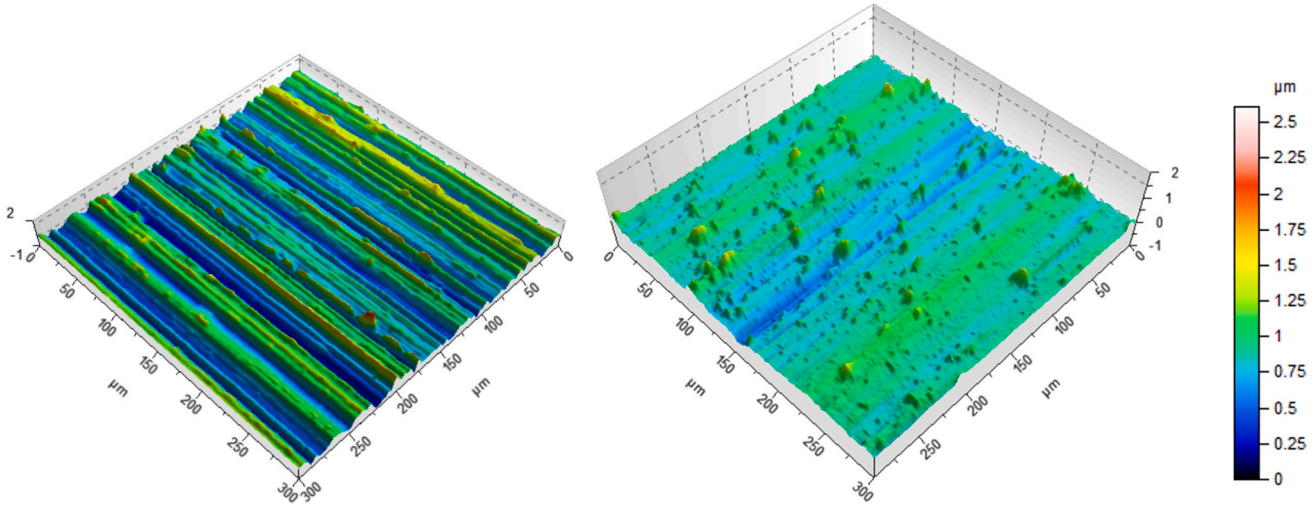

Fig. 7. Surface topographical map of bare-800grit (left) and bare-4000grit (right) 7075-T6, recorded by profilometry.

texturing of the material (see Fig. 7). The 4000grit_7075 exhibits the highest skewness of around 1.13, which is considerably higher than 4000grit_ AA2024-T3 with a S_{sk} of merely 0.38. Subsequent treatment of the 4000grit_ AA2024-T3 results in an increase of the S_{sk}, ranging from 0.52 (DI) to 0.79 (KOH), whereas treatment of 4000grit_AA075-T6 results in a decrease in S_{sk}. Lowest values are obtained after HNO_3 (0.52) and KOH (0.53) and slightly higher skewness for the DI-treated surface (0.90).

Considering the above, it can be concluded that the subsequent chemical treatments of AA7075-T6 result in an increase of the S_a but with a decrease of the S_{sk}, implying that while the surface is becoming rougher overall, the extreme variations in height are being reduced or evened out. In combination, this leads to a more normal height distribution along the roughness profile. For the AA2024-T3 substrate, an opposite trend is observed; S_a is decreased while S_{sk} values are increased. However, the relative changes of both S_{sk} and S_a are limited.

Since the trend for the calculated OH-fraction and 3D roughness (S_a) of differently pre-treated samples shows similar trends, it would be difficult to distinguish between the individual contributions of these two parameters on interfacial adhesion. Therefore, an additional set of samples was ground up to 800grit, and 3D surface topography was assessed (Fig. 8 c and d). As a result of much more severe abrasive conditions, all recorded S_a values were higher than the 4000grit specimens (Fig. 8 a and c). For 800grit_AA2024-T3, the roughness is 0.26 µm. After HNO_3, KOH and boiling DI water pre-treatments, no significant changes of the S_a from the 800grit_ AA2024-T3 are observed.

The S_a of 800grit_7075 is slightly higher than 800grit_AA2024-T3 at around 0.33 µm. Similarly, for this substrate, the difference in S_a after the different pre-treatments is not significant. Thus, no clear influence or trend was observed, distinguishing between the types of pre-treatments

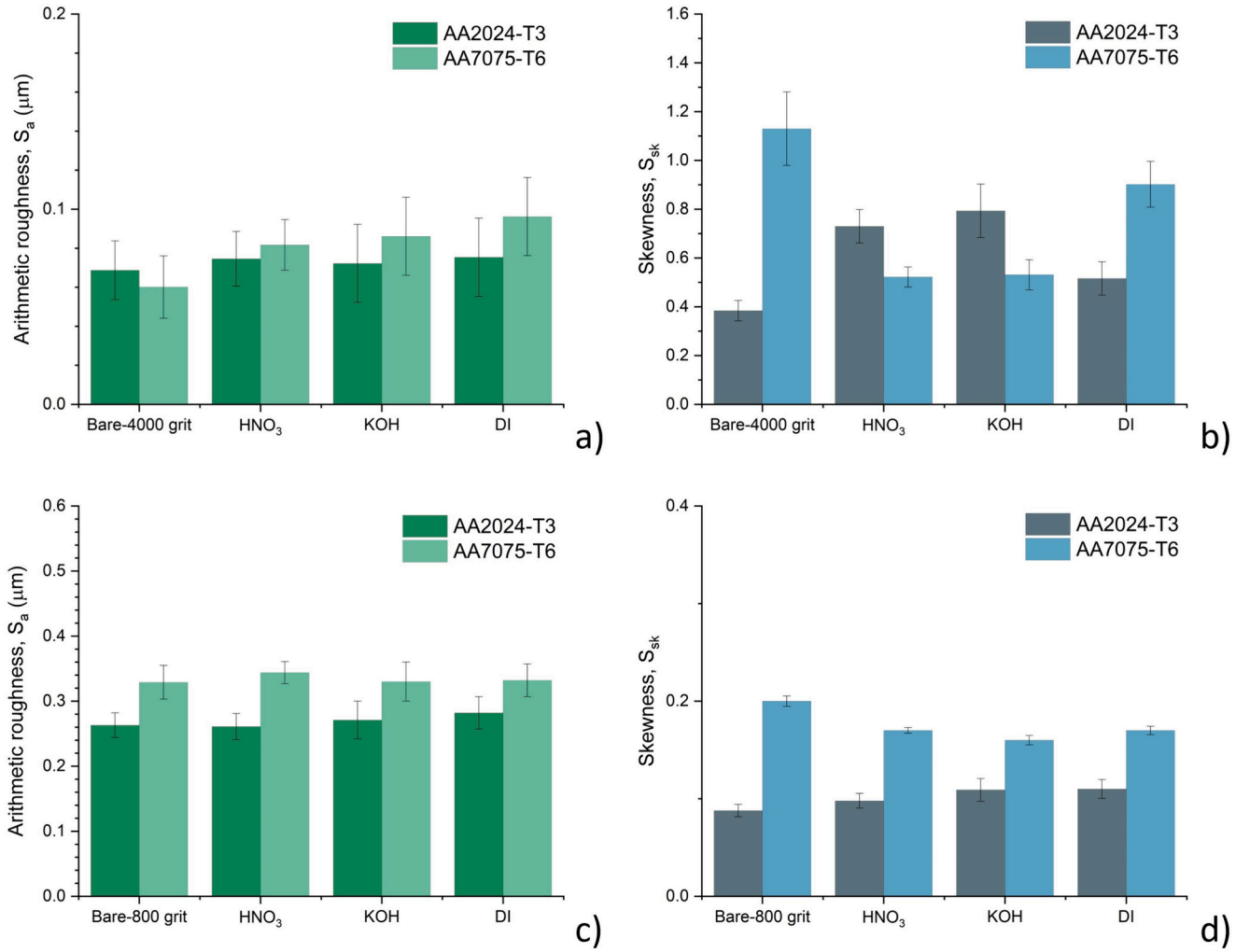

Fig. 8. The 3D arithmetic roughness, S_a and skewness, S_{sk} of differently pre-treated alloys. Bar charts (a-d) display S_a and S_{sk} values obtained from profilometry for alloys ground to 4000 grit or 800 grit.

on the coarsely abraded substrates.

The skewness of the AA7075-T6 alloy is 0.20 for the bare 800grit specimen, and subsequent treatment of the surface induces in all three cases a lowering of the skewness to around 0.17. For the AA2024-T3, the bare surface has a skewness of 0.09, and pre-treatment gives an increase to around 0.10 for all treatments. So, for the S_{sk} a similar absence of

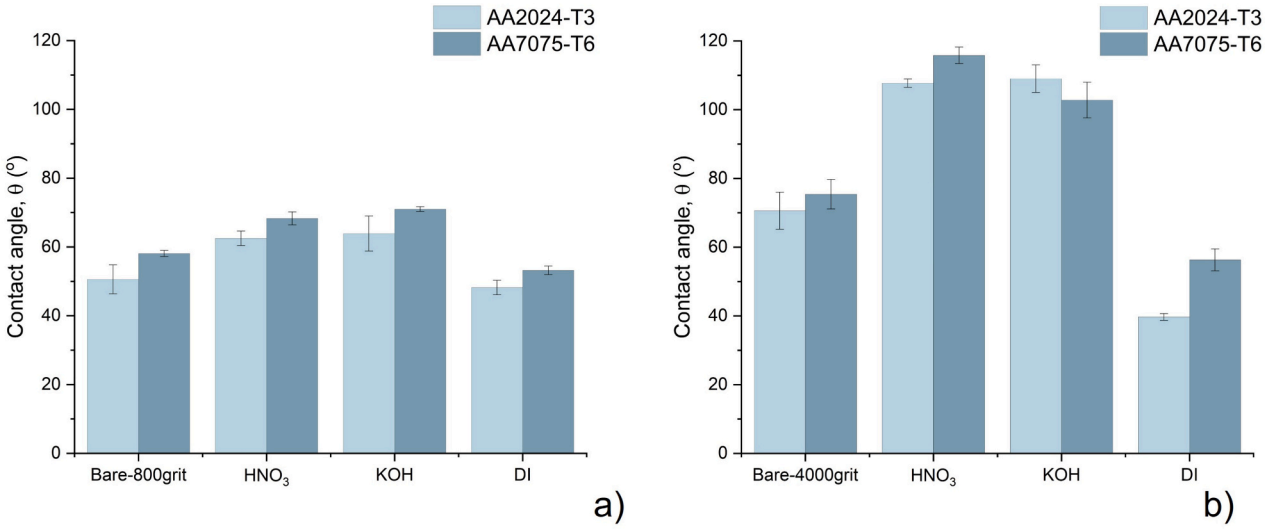

Fig. 9. Water contact angles of differently pre-treated AA2024 and AA7075 ground up to 800 grit (a) and 4000 grit (b).

alteration is observed as for the S_a, with all skewness values being very close to zero. The latter describing a normal symmetric distribution of the roughness before and after all treatments. Unlike the effect of pre-treatment for the finely abraded specimens, it is clear from roughness measurements that the pre-treatments induce non-significant morphological changes to the surfaces.

3.4. Surface wettability

Static water contact angles were measured to evaluate the wettability of the AA2024-T3 and AA7075-T6 surfaces after different pre-treatments. Fig. 9 presents the average static water contact angles of 4000grit_AA2024-T3 and 4000grit_AA7075-T6 before and after HNO_3, KOH and boiling DI water pre-treatments. The surface of 4000grit_AA2024-T3 is hydrophilic with a water contact angle of 71°. After HNO_3 and KOH pre-treatment the water contact angle increases to 108° and 109° respectively, and the surfaces have become hydrophobic. Unlike the aforementioned, DI boiling water treatment leads to a contact angle decrease to 40°, thereby increasing the hydrophilicity. The average static water contact angle of 4000grit_7075 is 75°. As was observed for AA2024-T3, the surface becomes hydrophobic after HNO_3 and KOH pre-treatments, with average contact angles of 116° and 103°. Similarly, boiling DI water decreases the water contact angle of AA7075-T6 to 53° and turns the surface hydrophilic.

The 800grit surfaces show a different wetting behaviour compared to the 4000grit surfaces. Both bare samples exhibit significantly lower static water contact angles of 51° and 58° for AA2024-T3 and AA7075-T6, respectively. The hydrophilicity has been enhanced due to the increased surface roughness of both surfaces. It can be noticed from the graphs in Fig. 9 that a similar trend is visible in the 800grit and 4000grit series; both HNO_3 and KOH treatments cause an increase in the water contact angle, while the DI water treatment results in a reduction of the water contact angle. However, in the case of the 800grit series, the water contact angles of all surfaces remain below 90°, remaining hydrophilic.

The wettability can be influenced by alterations in surface chemistry, e.g., by chemical modification of the surface, or by changing the surface morphology, e.g., by forming structures on the surface [24]. Both alkaline and acid treatments resulted in a hydrophobic surface on the aluminium alloys. The overall limited degree of surface roughness on the 4000 grit samples, coupled with the significant changes in roughness and surface morphology induced by the two treatments, suggests a strong influence of both surface chemistry alterations and changes in surface topography on the wetting behaviour. Both treatments cause an enrichment or increase in surface oxides, possibly leading to the observed shift to a hydrophobic surface. Additionally, both acid and alkaline treatments induce a micro-porosity at the surface, facilitating a transition from hydrophilic to hydrophobic behaviour as described by the Cassie-Baxter model (Fig. 3 and Table 3) [33,55,87–90]. At the same time, the increased hydrophilicity after DI water treatment is due to the higher wettability of the relative oxides present on the surface, pseudo-boehmite versus Al_2O_3, respectively [91].

Within the same reasoning, the 800grit samples show a smaller degree of change in surface roughness, and therefore, the surface chemistry is predominantly governing the wetting behaviour. Since a similar trend is observed for both the 4000grit and 800grit series, it can be concluded that the relative increases (HNO_3, KOH) and decrease (DI) of water contact angles are predominantly governed by chemical modification of the surface and, to a limited extent by the induced micro-porosity or pin-hole formation.

3.5. Adhesion

The silane-based hybrid sol-gel coating with incorporated cerium nitrate, was deposited on the differently pre-treated aluminium alloys, and its adhesion was assessed using pull-off testing. The effect of the HNO_3, KOH and DI boiling water pre-treatments on the adhesion of the sol-gel to the surfaces was assessed, and the adhesion was tested by applying an epoxy-based adhesive as top-film. The epoxy-silane of the sol-gel contains a reactive organic group for bonding to the adhesive [92]. Since the adhesion at the sol-gel/epoxy-based adhesive interface is considered the same for all treated samples, it can be inferred that the differences in adhesion are a direct result of interactions at the sol-gel/metal interface.

The average adhesion failure strengths (pull-off strengths) of the 4000grit specimens are presented in Fig. 10. For 4000grit_AA2024-T3, the average pull-off strength without applying the sol-gel is 5.3 MPa. The average pull-off strength increases by 28 % to 6.8 MPa after sol-gel application on the 4000grit_AA2024-T3. The HNO_3 treatment in combination with sol-gel application on AA2024-T3 (HNO_3 + SG) does not result in an additional increase, with similar adhesion values (6.7 MPa) as the bare+SG. Alkaline treatment with sol-gel (KOH + SG) gives a failure strength of 9.1 MPa, whereas DI + SG leads to an average failure strength of 14.2 MPa, which is more than twice the adhesion strength obtained after bare+SG. This clearly demonstrates the effect of surface pre-treatment on the adhesion of the sol-gel to the aluminium alloy substrate.

The pull-off strength of 4000grit_7075 was similar to the 4000grit_AA2024-T3, at 4.9 MPa. The application of the sol-gel showed a vast increase with 67 % to 8.2 MPa. The HNO_3, KOH and DI treatments in combination with sol-gel applications, all resulted in a further increase of the average failure strengths of 9.3, 11.2 and 13.2 MPa, respectively. The relative increase of combined DI treatment and sol-gel application is +169 % compared to 4000grit_AA7075-T6, which is nearly identical to the relative increase after DI + SG on AA2024-T3 (+168 %).

The results clearly show that applying sol-gel coating increases the adhesion with the epoxy-based adhesive for both substrates, AA2024 (28 %) and AA7075 (67 %), compared to bare4000grit samples. Furthermore, a clear effect of surface pre-treatment on sol-gel adhesion is shown.

Fractured surfaces after pull-off tests were studied to determine failure modes in the multi-layered system, consisting of interfaces between the substrate and the sol-gel coating and between the sol-gel coating and the epoxy-based adhesive. Fig. 11 presents images of the fractured surfaces of untreated and differently pre-treated AA2024-T3. Images of all fractured surfaces are supplied in the Supplementary information. The bare 4000grit_AA2024-T3 without sol-gel (Fig. 11a) shows a clean surface due to a full adhesive failure at the adhesive-substrate interface. Remnants of sol-gel on the fractured surfaces of the bare and HNO_3 samples indicate a mixture of adhesive failure at both the sol-gel/aluminium interface and failure in one of the parent layers or interfaces (Fig. 11b/c). The sol-gel-treated KOH pre-treated surface shows a lack of discolorations. At the edges, the multi-layer system failed cohesively within the adhesive and subsequently transitioned to an adhesive failure mode at the sol-gel/adhesive interface. This feature indicates that interfacial adhesion between substrate and sol-gel has improved and that the failure mode deviates from sol-gel/metal interfacial failure (Fig. 11d). Systems that obtain pull-off strengths higher than 9 MPa exhibit a transition to mixed or full cohesive failure within the epoxy adhesive, indicated by adhesive remnants on the fractured surface (Fig. 11d/e).

The improved adhesion can be attributed to the alterations in surface composition and associated OH-fraction, improved wetting, increased surface roughness or a combination of the aforementioned. In order to distinguish between the individual contributions of surface texture (roughness) and the other parameters, surfaces with higher surface roughness (800grit) and the same pre-treatments were also assessed in terms of adhesion. Fig. 10 as well shows the average adhesion failure strengths (pull-off strengths) of the 800grit series. Adhesion values obtained on the 800grit series demonstrate a similar trend as is observed for the 4000grit series in Fig. 10. For the 800grit samples, no significant topographical changes (as derived from the roughness values in Fig. 8 were induced by the surface treatments, as was the case for the 4000grit

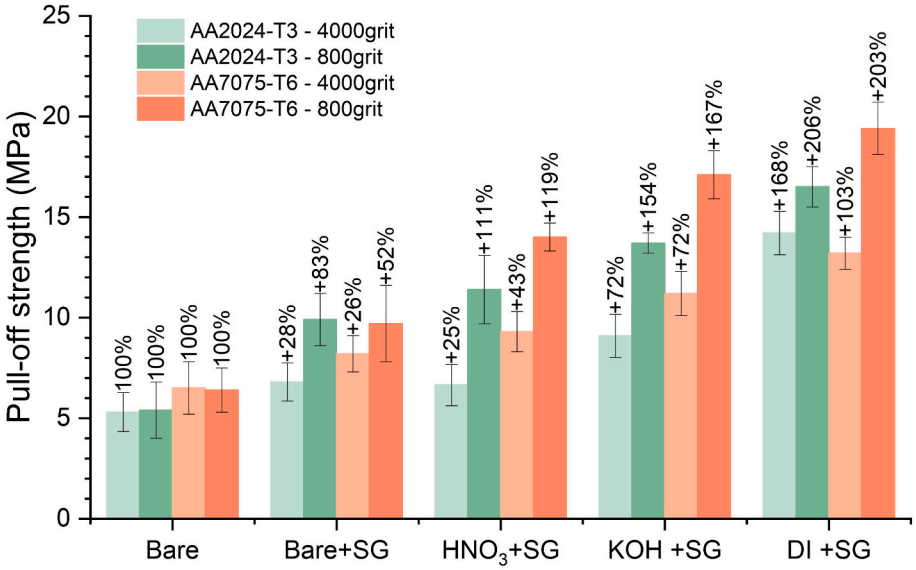

Fig. 10. Average adhesion strength (pull-off strength) of differently prepared AA2024-T3 and 7075-T6 aluminium alloys. Substrates were ground to either 4000 or 800 grit, with Araldite epoxy-based adhesive deposited on all surfaces. SG denotes sol-gel coatings, with percentages indicating the relative increases in adhesion strength compared to bare substrates with equal grit.

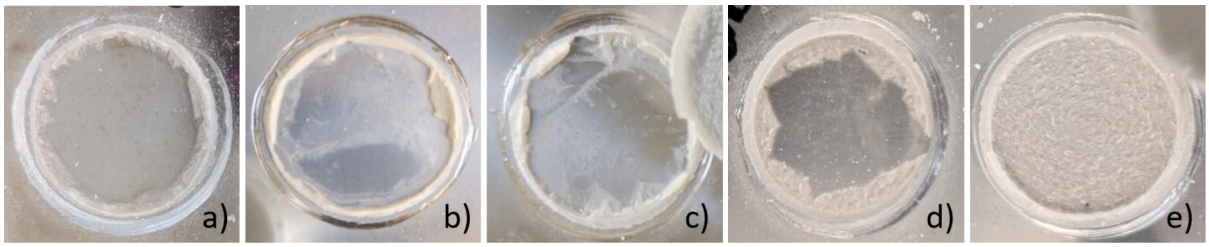

Fig. 11. Adhesion failure mode after pull-off test of AA2024-T3-4000grit - bare (a), bare+SG (b), HNO_3 + SG (c), KOH + SG (d) and DI + SG (e).

samples. The pull-off strength of bare-800grit is 5.4 MPa, comparable to the bare-4000grit AA2024-T3. After sol-gel application, a fracture strength of 9.9 MPa is recorded, an increase of +4.5 MPa (+83 %) compared to the bare-800 AA2024-T3. The HNO_3, KOH and DI pre-treatments followed by sol-gel application result in relative increases of adhesion strengths of +111 %, +154 % and + 206 %, leading to failure strengths of 11.4, 13.7 and 16.5 MPa, respectively. The overall trend is similar to the 4000grit samples, apart from the response to the HNO_3 treatment, but with higher values. The pull-off strength of bare 800grit_AA2024-T3 is 5.3, which is comparable with bare 4000grit_AA2024-T3.

The pull-off strength of bare 800grit_7075 is 6.4 MPa, which is somewhat higher than for the bare 4000grit_7075, which had an adhesion strength of 4.9 MPa. However, the trend of adhesion strengths after subsequent pre-treatments is similar to the 4000grit series. The application of the sol-gel on the rough surface leads to a relative increase of 52 % to 9.7 MPa. After the pre-treatments HNO_3, KOH and DI water in combination with the sol-gel coating, increases of adhesion strength of 119 %, 167 % and 203 % are observed. All adhesion strength values obtained after sol-gel application on the rougher surfaces are higher compared to the 4000grit series. All chemical pre-treatments lead to an improvement of the increase of the adhesion relative to the bare surface, compared to the 4000grit series. The pre-treatment with boiling DI water exhibits the highest adhesion values on all samples, which aligns with the findings on finely ground specimens (Fig. 10).

3.6. Statistical analysis

The differences in adhesion between the sol-gel and the aluminium alloy surfaces as a function of surface pre-treatment can be attributed to many surface properties; surface composition and associated OH-fraction, wetting behaviour, surface roughness or a combination of those. In order to evaluate the effect of different pre-treatments and associated OH-fractions, S_a, CA and adhesion, the obtained values were compared to a baseline scenario – bare substrate (before any pre-treatment and without sol-gel coating application). The effect of the different treatments was expressed as the relative increase (%) of the individual variables.

In Fig. 12, the relationship between the relative increases of Sa, CA and OH, and the relative increase of adhesion values are shown. From the regression of the distribution of all variables, Sa, CA, OH- and adhesion, it can be seen that the relation between OH and adhesion approaches linearity, while the relation between S_a, CA and adhesion does not. This gives a confirmation of the pre-dominant effect of surface chemistry versus surface roughness and surface wettability on the adhesion.

In order to conclude whether the obtained results show significant differences and to determine the correlations between all measured variables (OH-fraction, S_a, CA and adhesion), a complementary statistical analysis was performed. The correlations between the relative increases of OH-fraction, Sa, CA and adhesion were assessed using a Pearson's correlation and the significance is expressed by the p-value ($p < 0.01$). The obtained values from the Pearson's correlation coefficient matrix (r) and p-value statistics ($p < 0.01$) are presented in Table 5 and

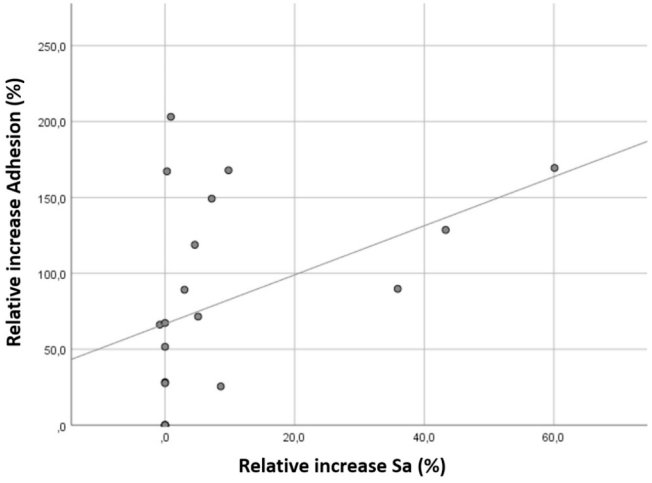

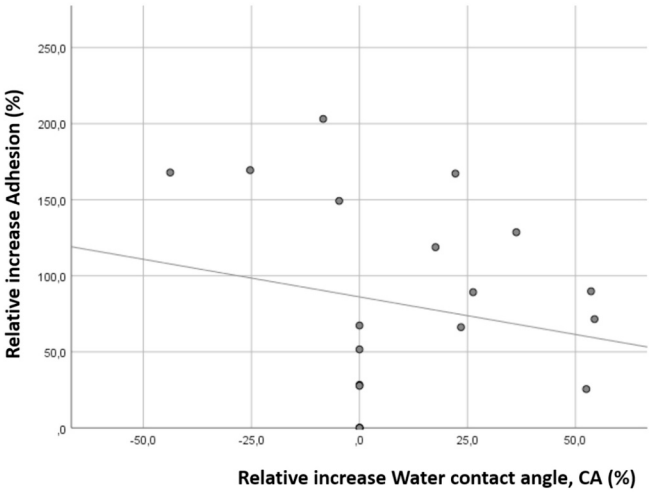

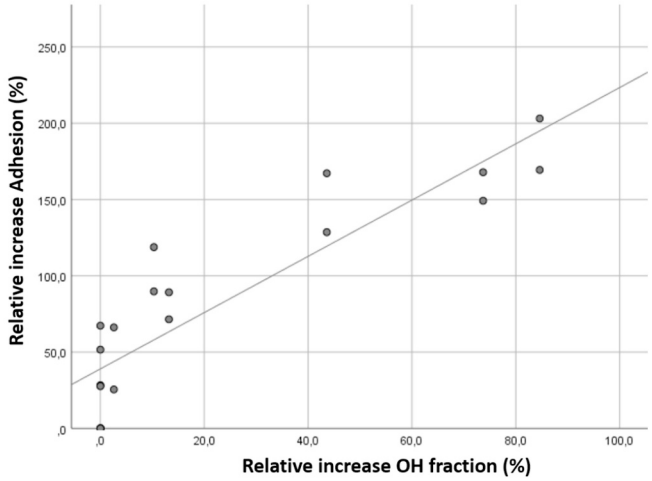

Fig. 12. Relationship between relative increases of S_a, CA and OH, and the adhesion strength.

Table 6, respectively. Overall, the measured samples, including both roughness series (4000 grit and 800 grit), a significant pairwise correlation was found for OH and adhesion indicated by $r = 0.89$ and a p-value of $1{,}67{\cdot}10^{-7}$, which is « 0.01. All other variables gave a non-significant pairwise correlation with the adhesion. Based on the statistical analysis performed, it can therefore be concluded that only the OH is directly related to the obtained adhesion strengths due to the strong pairwise correlation.

Table 5
Pearson pairwise correlation coefficients (r) for all variables of all tested specimens.

Pearson correlation coefficient (r)	Sa	CA	OH	Adhesion
Sa	1	0.07	0.47*	0.42
CA	0.07	1	−0.42	−0.19
OH	0.47*	−0.42	1	0.89**
Adhesion	0.42	−0.19	0.89**	1

* Correlation is significant at the 0.05 level (2-tailed).
** Correlation is significant at the 0.01 level (2-tailed).

Table 6
p-value of pairwise significance for all variables of tested specimens.

p-value	Sa	CA	OH	Adhesion
Sa	/	$7.75{\cdot}10^{-1}$	$3.70{\cdot}10^{-2}$	$6.80{\cdot}10^{-2}$
CA	$7.75{\cdot}10^{-1}$	/	$6.39{\cdot}10^{-2}$	$4.16{\cdot}10^{-1}$
OH	$3.70{\cdot}10^{-2}$	$6.39{\cdot}10^{-2}$	/	$1.67{\cdot}10^{-7}$
Adhesion	$6.80{\cdot}10^{-2}$	$4.16{\cdot}10^{-1}$	$1.67{\cdot}10^{-7}$	/

3.7. Overall discussion on the interweaving effects of various treatments

The two alloys exhibit distinct responses when subjected to the three different chemical pre-treatment methods. Discrepancies between the two alloys and the treatments are evident both in terms of the surface texture and surface chemical composition. For the adhesion study of the systems with sol-gel, again, large variations in the responses are observed. It can be seen that the two alloys show different trends in adhesion strengths as a function of pre-treatments. This implies that the final adhesion is indeed influenced by the surface conditions resulting from varying responses to the pre-treatment processes.

In addition, there are significant differences in the magnitude of the adhesion strength of the different systems. The results show undisputedly that the application of sol-gel coatings results in an improvement of the dry adhesion. However, the relative increase is again different for each substrate. What becomes distinctly evident from the outcomes of the adhesion tests is the pivotal role of the pre-treatment in facilitating the sol-gel's function as an adhesion promoter. The 'aggressive' acid and alkaline treatments lead to a more inhomogeneous response of the surfaces. This is because it is highly dependent on which alloying elements and phases are present in the alloy. These entities can react and interact with the surrounding matrix completely differently under the different conditions. The intrinsic susceptibility and electrochemical coupling of IMPs with the matrix can lead to local reactions. This mainly has a strong influence on surface chemistry. The selective dissolution of elements or the re-deposition of, for example, copper-rich oxides can bring about a significant change in surface chemistry. This, in turn, significantly affects the reaction of the sol-gel with the metal substrate. These locally widely varying responses to pre-treatment also affect surface morphology at the sub-micron scale. Local etching or leaching of phases or the deposition or growth of oxides can all lead to a strong change in surface texture but also determine the surface morphology. However, this effect is negligible on the surfaces with an initial high surface roughness. Local reactions at the surface still occur, however, they are irrelevant compared to the order of magnitude of the initial roughness. Nevertheless, the trend in terms of adhesion appears to be unchanged for the rough surfaces (800-grit) with respect to the surfaces with low surface roughness (4000-grit). This suggests that the surface chemistry, and thus the subsequent interactions at the sol-gel/metal interface, predominantly determines the strength of adhesion.

When one considers the responses of the two alloys to the acid and alkaline treatment, the effect of the microstructural complexity becomes

apparent. Both treatments result in copper enrichment on surfaces of AA7075-T6 as well as AA2024-T3 alloys, which is a phenomenon prevalently observed [80,81,93,94].

In the case of the thermochemical treatment with DI water, the response due to microstructural complexity is much less determinative. The treatment itself is less harsh in nature and mainly results in the growth of surface (hydr)oxides. These oxides have a relatively high hydroxyl or OH-fraction, which can be traced back to the formation of pseudo-boehmite [95]. Specifically, this high OH-fraction has a strong correlation with the adhesion and appears to be the determining parameter. This statement is supported by the statistical analysis, which shows a strong pairwise correlation between the OH-fraction and the obtained increase in adhesion, while no significant correlation was found for the surface roughness.

It's important to note that increasing the surface roughness of the bare samples, achieved by grinding to 800grit instead of 4000grit, did not result in a significant increase in adhesion strength. Some researchers have explained this phenomenon by stating that there exists a threshold value of roughness, beyond which further increases have no additional effect on adhesion for a specific combination of materials [96–98].

However, it can be clearly seen that both subsequent sol-gel application and the chemical treatments had a more prominent effect on adhesion than when applied to the fine 4000grit specimens. That is, both the absolute values in bond strength and the relative increases compared to the bare samples are a factor higher on the 800grit surfaces. Since the relative changes in surface roughness due to chemical treatment are not significant on the coarser 800-grit samples, two conclusions can be drawn. Either the micro texture on the surface has a greater influence than the macro texture, or the 800-grit samples, with their higher degree of texture, offer a larger relative surface area. The relatively larger surface subsequently provides a significantly higher number of sites for chemical changes to occur, thereby causing any enhancing effect of the chemical alteration after a pre-treatment to be more profound [70,99].

As a final note, while our study explored the role of alloying elements, the precise contribution of the intermetallics remains unclear. Further localized spectroscopic and microscopic analyses are necessary to clarify this aspect, which holds significance for future research in this field.

4. Conclusions

The complex interplay of surface chemistry, morphology, wettability, and adhesion within these materials was elucidated through this investigation. The response of aluminium alloys AA2024-T3 and 7075-T6 to three distinct pre-treatments, namely HNO_3 (acid), KOH (alkaline), and boiling DI water (thermochemical), unveils important insights into their surface behaviour and subsequent correlation to interfacial sol-gel adhesion.

It was found that the response in terms of surface chemical composition is profoundly influenced by the alloying elements and their intermetallic phases, thereby determining the outcome of the pre-treatments. Acid and alkaline treatments, while inducing non-uniform surface responses, stand out for causing the most pronounced changes in overall surface chemical composition. This phenomenon is accompanied by marked variations in surface morphology and texture, particularly prominent following the acid and alkaline treatments. In contrast, the thermochemical treatment involving DI water yields a moderate effect on surface chemistry due to its more uniform surface response. The thermochemical treatment stands out for promoting the formation of surface oxides with the highest hydroxyl fraction.

Additionally, the pre-treatments exert distinct effects on the wetting behaviour of the aluminium alloy surfaces. Nevertheless, this parameter does not directly correlate with the measured sol-gel adhesion. However, a direct correlation was found between the hydroxyl fraction, as determined by XPS-analysis, and the adhesion strength of the sol-gel coating. Interestingly, the surface roughness failed to exhibit a significant correlation with adhesion.

In summary, the interaction between the material's alloy composition and microstructural constituents plays a pivotal role in determining surface responses to surface treatment and subsequent adhesion of superimposed layers.

CRediT authorship contribution statement

J.P.B. van Dam: Writing – review & editing, Writing – original draft, Validation, Methodology, Investigation, Formal analysis, Data curation, Conceptualization. **U. Tiringer:** Writing – review & editing, Writing – original draft, Methodology, Investigation, Formal analysis, Data curation, Conceptualization. **S.T. Abrahami:** Writing – review & editing, Validation, Investigation, Formal analysis. **I. Milošev:** Writing – review & editing, Validation, Investigation, Formal analysis. **H. Terryn:** Writing – review & editing, Supervision, Methodology, Conceptualization. **J. Kovač:** Writing – review & editing, Validation, Investigation, Formal analysis. **J.M.C. Mol:** Writing – review & editing, Supervision, Resources, Funding acquisition, Conceptualization.

Declaration of competing interest

The authors declare that they have no known competing financial interests or personal relationships that could have appeared to influence the work reported in this paper.

Data availability

Data will be made available on request.

Acknowledgements

This work was supported by the European Union's Horizon 2020 Research and Innovation Programme under the Marie Skłodowska-Curie Grant agreement No. 707404. J.P.B.D. acknowledges financial support by Materials Innovation Institute M2i and Technology Foundation TTW (www.stw.nl), which is part of the Netherlands Organization for Scientific Research under project number S32.4.14552b. Special thanks are extended to M.I. Hoppen for their invaluable assistance with the statistical analysis.

Appendix A. Supplementary data

Supplementary data to this article can be found online at https://doi.org/10.1016/j.surfcoat.2024.130901.

References

[1] W. Brockmann, P.L. Geiß, J. Klingen, B. Schröder, Adhesive bonding as a joining technique, Adhes. Bond Mater. Appl. Technol. (2009) 1–3.
[2] A. Higgins, Adhesive bonding of aircraft structures, Int. J. Adhes. Adhes. 20 (2000) 367–376, https://doi.org/10.1016/S0143-7496(00)00006-3.
[3] F. Cavezza, M. Boehm, H. Terryn, T. Hauffman, A review on adhesively bonded aluminium joints in the automotive industry, Metals (Basel) 10 (2020) 1–32, https://doi.org/10.3390/met10060730.
[4] N.L. Sukiman, X. Zhou, N. Birbilis, A.E. Hughes, J.M.C. Mol, S.J. Garcia, et al., Durability and corrosion of aluminium and its alloys: overview, property space, techniques and developments, Alum. Alloy Trends Fabr. Appl. 5 (2012) 47–97.
[5] A.E. Hughes, N. Birbilis, J.M.C. Mol, S.J. Garcia, X. Zhou, G.E. Thompson, et al., High strength Al-alloys: microstructure, corrosion and principles of protection, Recent Trends Process Degrad Alum Alloy 1 (2011) 223–262, https://doi.org/10.5772/18766.
[6] S.J. Garcia, T.A. Markley, J.M.C. Mol, A.E. Hughes, Unravelling the corrosion inhibition mechanisms of bi-functional inhibitors by EIS and SEM-EDS, Corros. Sci. 69 (2013) 346–358, https://doi.org/10.1016/j.corsci.2012.12.018.
[7] B. Zhou, B. Liu, S. Zhang, R. Lin, Y. Jiang, X. Lan, Microstructure evolution of recycled 7075 aluminum alloy and its mechanical and corrosion properties, J. Alloys Compd. 879 (2021) 160407, https://doi.org/10.1016/j.jallcom.2021.160407.

[8] A.E. Hughes, C. MacRae, N. Wilson, A. Torpy, T.H. Muster, A.M. Glenn, Sheet AA2024-T3: a new investigation of microstructure and composition, Surf. Interface Anal. 42 (2010) 334–338, https://doi.org/10.1002/sia.3163.

[9] J. Cerezo, I. Vandendael, R. Posner, J.H.W. de Wit, J.M.C. Mol, H. Terryn, The effect of surface pre-conditioning treatments on the local composition of Zr-based conversion coatings formed on aluminium alloys, Appl. Surf. Sci. 366 (2016) 339–347, https://doi.org/10.1016/j.apsusc.2016.01.106.

[10] A. Matei, O. Tutunaru, V. Tucureanu, Surface pre-treatment of aluminum alloys for the deposition of composite materials, Mater. Sci. Eng. B Solid-State Mater. Adv. Technol. 263 (2021) 114874, https://doi.org/10.1016/j.mseb.2020.114874.

[11] A.F. Carreira, A.M. Pereira, E.P. Vaz, A.M. Cabral, T. Ghidini, L. Pigliaru, et al., Alternative corrosion protection pretreatments for aluminum alloys, J. Coatings Technol. Res. 14 (2017) 879–892, https://doi.org/10.1007/s11998-017-9922-9.

[12] A. Boag, A.E. Hughes, A.M. Glenn, T.H. Muster, D. McCulloch, Corrosion of AA2024-T3 part I: localised corrosion of isolated IM particles, Corros. Sci. 53 (2011) 17–26, https://doi.org/10.1016/j.corsci.2010.09.009.

[13] N. Birbilis, Y.M. Zhu, S.K. Kairy, M.A. Glenn, J.-F. Nie, A.J. Morton, et al., A closer look at constituent induced localised corrosion in Al-Cu-Mg alloys, Corros. Sci. 113 (2016) 160–171.

[14] C. Vargel, M. Jacques, M.P. Schmidt, Corrosion of Aluminium, 1st ed., Elsevier, Amsterdam, the Netherlands, 2004.

[15] J.R. Davis, Corrosion of Aluminum and Aluminum Alloys, Asm International, 1999.

[16] N. Birbilis, R.G. Buchheit, Investigation and discussion of characteristics for intermetallic phases common to aluminum alloys as a function of solution pH, J. Electrochem. Soc. 155 (2008) C117.

[17] N. Birbilis, R.G. Buchheit, Electrochemical characteristics of intermetallic phases in aluminum alloys, J. Electrochem. Soc. 152 (2005) B140, https://doi.org/10.1149/1.1869984.

[18] I. Milošev, P. Rodič, Cerium chloride and acetate salts as corrosion inhibitors for aluminum alloy AA7075-T6 in sodium chloride solution, Corrosion 72 (2016) 1021–1034.

[19] P. Rodič, I. Milošev, Corrosion inhibition of pure aluminium and alloys AA2024-T3 and AA7075-T6 by cerium (III) and cerium (IV) salts, J. Electrochem. Soc. 163 (2015) C85.

[20] S.T. Abrahami, T. Hauffman, J.M.M. de Kok, J.M.C. Mol, H. Terryn, Effect of anodic aluminum oxide chemistry on adhesive bonding of epoxy, J. Phys. Chem. C 120 (2016) 19670–19677, https://doi.org/10.1021/acs.jpcc.6b04957.

[21] S.Y. Park, W.J. Choi, B.C. Yoon, Analysis of effects of process factors on corrosion resistance of adhesive bonded joints for aluminum alloys, J. Mater. Process. Technol. 276 (2020) 116412, https://doi.org/10.1016/j.jmatprotec.2019.116412.

[22] L.I. Fockaert, P. Taheri, S.T. Abrahami, B. Boelen, H. Terryn, J.M.C. Mol, Zirconium-based conversion film formation on zinc, aluminium and magnesium oxides and their interactions with functionalized molecules, Appl. Surf. Sci. 423 (2017) 817–828, https://doi.org/10.1016/j.apsusc.2017.06.174.

[23] S.T. Abrahami, T. Hauffman, J.M.M. De Kok, J.M.C. Mol, H. Terryn, XPS analysis of the surface chemistry and interfacial bonding of barrier-type Cr(VI)-free anodic oxides, J. Phys. Chem. C 119 (2015) 19967–19975, https://doi.org/10.1021/acs.jpcc.5b05958.

[24] S.T. Abrahami, J.M.M. de Kok, H. Terryn, J.M.C. Mol, Towards Cr(VI)-free anodization of aluminum alloys for aerospace adhesive bonding applications: a review, Front. Chem. Sci. Eng. 11 (2017) 465–482, https://doi.org/10.1007/s11705-017-1641-3.

[25] S. Pletincx, K. Marcoen, L. Trotochaud, L.I. Fockaert, J.M.C. Mol, A.R. Head, et al., Unravelling the chemical influence of water on the PMMA/aluminum oxide hybrid interface in situ, Sci. Rep. 7 (2017) 1–11, https://doi.org/10.1038/s41598-017-13549-z.

[26] J.M.C. Mol, B.R.W. Hinton, D.H. Van Der Weijde, J.H.W. De Wit, S. Van Der Zwaag, A filiform corrosion and potentiodynamic polarisation study of some aluminium alloys, J. Mater. Sci. 35 (2000) 1629–1639, https://doi.org/10.1023/A:1004795528090.

[27] O. Lunder, F. Lapique, B. Johnsen, K. Nisancioglu, Effect of pre-treatment on the durability of epoxy-bonded AA6060 aluminium joints, Int. J. Adhes. Adhes. 24 (2004) 107–117, https://doi.org/10.1016/j.ijadhadh.2003.07.002.

[28] J. Liu, M.K. Chaudhury, D.H. Berry, J.E. Seebergh, J.H. Osborne, K.Y. Blohowiak, Effect of surface morphology on crack growth at a sol-gel reinforced epoxy/aluminum interface, J. Adhes. 82 (2006) 487–516, https://doi.org/10.1080/00218460600713725.

[29] H.M.S. Iqbal, S. Bhowmik, R. Benedictus, Durability of PBI adhesive bonded joints under various environmental conditions, Int. J. Adhes. Adhes. 89 (2019) 154–160, https://doi.org/10.1016/j.ijadhadh.2019.01.006.

[30] A. Peetsch, C. Blaffert, C. Ramm, M. Renkel, R. O'Kane, B. Floryancic, et al., Novel chrome-free bonding primer for structural bonding and corrosion protection in aerospace applications, Int SAMPE Tech Conf 2021 (2021-June) 789–802, https://doi.org/10.33599/nasampe/s.21.0514.

[31] G.W. Critchlow, D.M. Brewis, Review of surface pretreatments for aluminium alloys, Int. J. Adhes. Adhes. 16 (1996) 255–275.

[32] S.S. Golru, M.M. Attar, B. Ramezanzadeh, S. Sharifi Golru, M.M. Attar, B. Ramezanzadeh, Effects of different surface cleaning procedures on the superficial morphology and the adhesive strength of epoxy coating on aluminium alloy 1050, Prog. Org. Coatings 87 (2015) 52–60, https://doi.org/10.1016/j.porgcoat.2015.05.005.

[33] I. Milošev, P. Rodič, The effect of surface pretreatment of aluminum alloy 7075-T6 on the subsequent inhibition by cerium(III) acetate in chloride-containing solution, J. Electrochem. Soc. 169 (2022) 011504, https://doi.org/10.1149/1945-7111/ac4933.

[34] A. Özdemir, İ. Kocabaş, P. Svanda, Improving the strength of adhesively bonded joints through the introduction of various surface treatments, J. Adhes. Sci. Technol. 30 (2016) 2573–2595, https://doi.org/10.1080/01694243.2016.1188872.

[35] A.E. Hughes, G. Theodossiou, S. Elliott, T.G. Harvey, P.R. Miller, J.D. Gorman, et al., Study of deoxidation of 2024-T3 with various acids, Mater. Sci. Technol. 17 (2001) 1642–1652, https://doi.org/10.1179/026708301101509728.

[36] L.E.M. Palomino, J.F.W. De Castro, I.V. Aoki, H.G. De Melo, Microstructural and electrochemical characterization of environmentally friendly conversion layers on aluminium alloys, J. Braz. Chem. Soc. 14 (2003) 651–659, https://doi.org/10.1590/S0103-50532003000400024.

[37] Y. Liu, M.A. Arenas, A. De Frutos, J. De Damborenea, A. Conde, P. Skeldon, et al., Influence of nitric acid pre-treatment on Al–Cu alloys, Electrochim. Acta 53 (2008) 4454–4460.

[38] S. Joshi, W.G. Fahrenholtz, OKeefe MJ., Effect of alkaline cleaning and activation on aluminum alloy 7075-T6, Appl. Surf. Sci. 257 (2011) 1859–1863, https://doi.org/10.1016/j.apsusc.2010.08.126.

[39] A. Baldan, Adhesively-bonded joints and repairs in metallic alloys, polymers and composite materials: adhesives, adhesion theories and surface pretreatment, J. Mater. Sci. 39 (2004) 1–49, https://doi.org/10.1023/B:JMSC.0000007726.58758.e4.

[40] S.T. Abrahami, T. Hauffman, J.M.M. de Kok, H. Terryn, J.M.C. Mol, The role of acid-base properties in the interactions across the oxide-primer interface in aerospace applications, Surf. Interface Anal. 48 (2016) 712–720, https://doi.org/10.1002/sia.5907.

[41] R. del Olmo, U. Tiringer, I. Milošev, P. Visser, R. Arrabal, E. Matykina, et al., Hybrid sol-gel coatings applied on anodized AA2024-T3 for active corrosion protection, Surf. Coatings Technol. 419 (2021) 127251, https://doi.org/10.1016/j.surfcoat.2021.127251.

[42] C. Trinidad, J. Światowska, S. Zanna, A. Seyeux, D. Mercier, R. Viroulaud, et al., Effect of surface preparation treatments on copper enrichment on 2024 aluminium alloy surface, Appl. Surf. Sci. (2021) 560, https://doi.org/10.1016/j.apsusc.2021.149991.

[43] J. Cerezo, P. Taheri, I. Vandendael, R. Posner, K. Lill, J.H.W. de Wit, et al., Influence of surface hydroxyls on the formation of Zr-based conversion coatings on AA6014 aluminum alloy, Surf. Coatings Technol. 254 (2014) 277–283, https://doi.org/10.1016/j.surfcoat.2014.06.030.

[44] S. Meyer, U. Schubert, M. De Bardi, R. Wiesinger, M. Schreiner, T. Grohmann, Adhesion pretreatment of aluminum by sol-gel processing, Int. J. Adhes. Adhes. 51 (2014) 103–110, https://doi.org/10.1016/j.ijadhadh.2014.02.015.

[45] Y.H. Han, A. Taylor, K.M. Knowles, Scratch resistance and adherence of novel organic-inorganic hybrid coatings on metallic and non-metallic substrates, Surf. Coatings Technol. 203 (2009) 2871–2877, https://doi.org/10.1016/j.surfcoat.2009.03.003.

[46] A. Suárez-Vega, C. Agustín-Sáenz, L.A. O'Dell, F. Brusciotti, A. Somers, M. Forsyth, Properties of hybrid sol-gel coatings with the incorporation of lanthanum 4-hydroxy cinnamate as corrosion inhibitor on carbon steel with different surface finishes, Appl. Surf. Sci. (2021) 561, https://doi.org/10.1016/j.apsusc.2021.149881.

[47] F. Maia, K.A. Yasakau, J. Carneiro, S. Kallip, J. Tedim, T. Henriques, et al., Corrosion protection of AA2024 by sol-gel coatings modified with MBT-loaded polyurea microcapsules, Chem. Eng. J. 283 (2016) 1108–1117, https://doi.org/10.1016/j.cej.2015.07.087.

[48] H. Chen, J. Shen, J. Deng, Y. Hu, Y. Zhang, Sol–gel coatings with hydrothermal hydroxylation as pre-treatment for 2198-T851 corrosion protection performance, Appl. Surf. Sci. 508 (2020) 145285, https://doi.org/10.1016/j.apsusc.2020.145285.

[49] A. Franquet, H. Terryn, J. Vereecken, Study of the effect of different aluminium surface pretreatments on the deposition of thin non-functional silane coatings, Surf. Interface Anal. 36 (2004) 681–684, https://doi.org/10.1002/sia.1735.

[50] J. Torras, D.S. Azambuja, J.M. Wolf, C. Alemán, E. Armelin, How organophosphonic acid promotes silane deposition onto aluminum surface: a detailed investigation on adsorption mechanism, J. Phys. Chem. C 118 (2014) 17724–17736, https://doi.org/10.1021/jp5046707.

[51] J.F. Watts, A. Rattana, M. Abel, Interfacial chemistry of adhesives on hydrated aluminium and hydrated aluminium treated with an organosilane, Surf Interface Anal An Int J Devoted to Dev Appl Tech Anal Surfaces, Interfaces Thin Film 36 (2004) 1449–1468.

[52] M. Abel, R.P. Digby, I.W. Fletcher, J.F. Watts, Evidence of specific interaction between γ-glycidoxypropyltrimethoxysilane and oxidized aluminium using high-mass resolution ToF-SIMS, Surf Interface Anal An Int J Devoted to Dev Appl Tech Anal Surfaces, Interfaces Thin Film 29 (2000) 115–125.

[53] C. Le Pen, B. Vuillemin, S. Van Gils, H. Terryn, R. Oltra, In-situ characterisation of organosilane film formation on aluminium alloys by electrochemical quartz crystal microbalance and in-situ ellipsometry, Thin Solid Films 483 (2005) 66–73.

[54] A.N. Rider, D.R. Arnott, Boiling water and silane pre-treatment of aluminium alloys for durable adhesive bonding, Int. J. Adhes. Adhes. 20 (2000) 209–220.

[55] A. Trentin, R. Samiee, A.H. Pakseresht, A. Duran, Y. Castro, D. Galusek, Influence of pre-treatments on adhesion, barrier and mechanical properties of epoxy coatings: a comparison between steel, AA7075 and AA2024, Appl. Surf. Sci. Adv. 18 (2023) 100479, https://doi.org/10.1016/j.apsadv.2023.100479.

[56] S.Y. Park, W.J. Choi, Investigation on the effectiveness of silane-based field level surface treatments of aluminum substrates for on-aircraft bonded repairs, Int. J. Adhes. Adhes. 95 (2019) 102414, https://doi.org/10.1016/j.ijadhadh.2019.102414.

[57] R.B. Figueira, C.J.R. Silva, E.V. Pereira, Organic–inorganic hybrid sol–gel coatings for metal corrosion protection: a review of recent progress, J. Coatings Technol. Res. 12 (2015) 1–35, https://doi.org/10.1007/s11998-014-9595-6.
[58] R.B. Figueira, I.R. Fontinha, C.J.R. Silva, E.V. Pereira, Hybrid sol-gel coatings: smart and green materials for corrosion mitigation, Coatings 6 (2016) 12, https://doi.org/10.3390/coatings6010012.
[59] R.B. Figueira, Hybrid sol–gel coatings for corrosion mitigation: a critical review, Polymers (Basel) 12 (2020) 689, https://doi.org/10.3390/polym12030689.
[60] M.L. Zheludkevich, R. Serra, M.F. Montemor, K.A. Yasakau, I.M.M. Salvado, M.G. S. Ferreira, Nanostructured sol-gel coatings doped with cerium nitrate as pre-treatments for AA2024-T3 corrosion protection performance, Electrochim. Acta 51 (2005) 208–217, https://doi.org/10.1016/j.electacta.2005.04.021.
[61] I.R. Fontinha, M.M. Salta, M.L. Zheludkevich, M.G.S. Ferreira, EIS study of amine cured epoxy-silica-zirconia sol-gel coatings for corrosion protection of the aluminium alloy EN AW 6063, Port. Electrochim. Acta 31 (2013) 307–319, https://doi.org/10.4152/pea.201306307.
[62] J.O. Iroh, D. Rajamani, Synthesis and structure of environmentally friendly hybrid clay/organosilane nanocomposite coatings, J. Inorg. Organomet. Polym. Mater. 22 (2012) 595–603.
[63] S.A.Z. Estekhraji, S. Amiri, Synthesis and characterization of anti-fungus, anti-corrosion and self-cleaning hybrid nanocomposite coatings based on sol–gel process, J. Inorg. Organomet. Polym. Mater. 27 (2017) 883–891.
[64] C. Chen, M. Yu, Z. Zhan, Y. Ge, Z. Sun, J. Liu, Effect of pH on the structure and corrosion protection properties of sol-gel coatings, Corros. Sci. 212 (2023) 110955, https://doi.org/10.1016/j.corsci.2022.110955.
[65] R. del Olmo, E. López, E. Matykina, U. Tiringer, J.M.C. Mol, M. Mohedano, et al., Hybrid PEO/sol-gel coatings loaded with Ce for corrosion protection of AA2024-T3, Prog. Org. Coatings 182 (2023) 1–16, https://doi.org/10.1016/j.porgcoat.2023.107667.
[66] O.M. Prada Ramirez, T.F. de Almeida, J.H. Marin, P.H. Suegama, M. Starykevich, M.G.S. Ferreira, et al., Effect of hydrolysis time on the corrosion resistance of sol-gel coated AA2024-T3 anodized in TSA, Surf. Coatings Technol. (2024) 482, https://doi.org/10.1016/j.surfcoat.2024.130683.
[67] O.M. Prada Ramirez, T.M. Kremmer, J.H. Marin, B.P. da Silva, M. Starykevich, M. A. Tunes, et al., Ce nanoparticles and sol-gel hybrid organic-inorganic coatings maximize corrosion protection in the anodized AA2024-T3, Corros. Sci. 221 (2023) 111330, https://doi.org/10.1016/j.corsci.2023.111330.
[68] J. Liu, M.K. Chaudhury, D.H. Berry, J.E. Seebergh, J.H. Osborne, K.Y. Blohowiak, Effect of processing conditions on adhesion performance of a sol-gel reinforced epoxy/aluminum interface, J. Adhes. Sci. Technol. 22 (2008) 1159–1180, https://doi.org/10.1163/156856108X312635.
[69] M. May, H. Wang, R. Akid, Bond strength of hybrid sol-gel coatings with different additives, J. Coatings Technol. Res. 10 (2013) 407–413, https://doi.org/10.1007/s11998-012-9450-6.
[70] U. Tiringer, J.P.B. van Dam, S.T. Abrahami, H. Terryn, J. Kovač, I. Milošev, J.M. C. Mol, et al., Scrutinizing the importance of surface chemistry versus surface roughness for aluminium / sol-gel film adhesion, Surf. Interfaces 26 (2021) 18–21, https://doi.org/10.1016/j.surfin.2021.101417.
[71] M. Fedel, F. Deflorian, Influence of a boiling water treatment on the electrochemical properties of a sol-gel film on AA1050, Trans. Inst. Met. Finish. 93 (2015) 313–320, https://doi.org/10.1080/00202967.2015.1117261.
[72] U. Tiringer, A. Durán, Y. Castro, I. Milošev, Self-Healing Effect of Hybrid Sol-Gel Coatings Based on GPTMS, TEOS, SiO 2 Nanoparticles and Ce(NO 3) 3 Applied on Aluminum Alloy 7075-T6, J. Electrochem. Soc. 165 (2018) C213–C225, https://doi.org/10.1149/2.0211805jes.
[73] U. Tiringer, B. Mušič, D. Zimerl, G. Šekularac, S. Stavber, I. Milošev, The effects of cerium ions on the curing, polymerisation and condensation of hybrid sol-gel coatings, J. Non Cryst. Solids 510 (2019) 93–100, https://doi.org/10.1016/j.jnoncrysol.2018.12.021.
[74] U. Tiringer, I. Milošev, A. Durán, Y. Castro, Hybrid sol–gel coatings based on GPTMS/TEOS containing colloidal SiO2 and cerium nitrate for increasing corrosion protection of aluminium alloy 7075-T6, J. Sol-Gel Sci. Technol. 85 (2018) 546–557, https://doi.org/10.1007/s10971-017-4577-7.
[75] E. McCafferty, J.P. Wightman, Determination of the concentration of surface hydroxyl groups on metal oxide films by a quantitative XPS method, Surf. Interface Anal. 26 (1998) 549–564, https://doi.org/10.1002/(sici)1096-9918(199807)26:8<549::aid-sia396>3.3.co;2-h.
[76] K.Y. Law, Definitions for hydrophilicity, hydrophobicity, and superhydrophobicity: getting the basics right, J. Phys. Chem. Lett. 5 (2014) 686–688, https://doi.org/10.1021/jz402762h.
[77] P. Schober, L.A. Schwarte, Correlation coefficients: appropriate use and interpretation, Anesth. Analg. 126 (2018) 1763–1768, https://doi.org/10.1213/ANE.0000000000002864.
[78] G. James, D. Witten, T. Hastie, R. Tibshirani, An Introduction to Statistical Learning: With Applications in R vol. 103, Springer New York, New York, NY, 2013, https://doi.org/10.1007/978-1-4614-7138-7.
[79] A. Kosari, F. Tichelaar, P. Visser, H. Zandbergen, H. Terryn, J.M.C. Mol, Dealloying-driven local corrosion by intermetallic constituent particles and dispersoids in aerospace aluminium alloys, Corros. Sci. 177 (2020) 108947, https://doi.org/10.1016/j.corsci.2020.108947.
[80] U. Tiringer, J. Kovač, I. Milošev, Effects of mechanical and chemical pre-treatments on the morphology and composition of surfaces of aluminium alloys 7075-T6 and 2024-T3, Corros. Sci. 119 (2017) 46–59, https://doi.org/10.1016/j.corsci.2017.02.018.
[81] A. de Frutos, M.A. Arenas, Y. Liu, P. Skeldon, G.E. Thompson, J. de Damborenea, et al., Influence of pre-treatments in cerium conversion treatment of AA2024-T3 and 7075-T6 alloys, Surf. Coatings Technol. 202 (2008) 3797–3807, https://doi.org/10.1016/j.surfcoat.2008.01.027.
[82] M. Witkowska, G.E. Thompson, T. Hashimoto, E. Koroleva, Assessment of the surface reactivity of AA1050 aluminium alloy, Surf. Interface Anal. 45 (2013) 1585–1589.
[83] E. Koroleva, G.E. Thompson, G. Hollrigl, M. Bloeck, Surface morphological changes of aluminium alloys in alkaline solution:: effect of second phase material, Corros. Sci. 41 (1999) 1475–1495.
[84] H. Zhan, J.M.C. Mol, F. Hannour, L. Zhuang, H. Terryn, J.H.W. De Wit, The influence of copper content on intergranular corrosion of model AlMgSi (Cu) alloys, Mater. Corros. 59 (2008) 670–675.
[85] M. Olgiati, P.J. Denissen, S.J. Garcia, When all intermetallics dealloy in AA2024-T3: quantifying early stage intermetallic corrosion kinetics under immersion, Corros. Sci. 192 (2021) 109836.
[86] T.R. Thomas, Rough Surfaces, Imperial College Press, London, 1999.
[87] I. Milošev, T. Bakarič, S. Zanna, A. Seyeux, P. Rodič, M. Poberžnik, et al., Electrochemical, surface-analytical, and computational DFT study of alkaline etched aluminum modified by carboxylic acids for corrosion protection and hydrophobicity, J. Electrochem. Soc. 166 (2019) C3131–C3146, https://doi.org/10.1149/2.0181911jes.
[88] M. Mrad, Y. Ben Amor, L. Dhouibi, M.F. Montemor, Effect of AA2024-T3 surface pretreatment on the physicochemical properties and the anticorrosion performance of poly(γ-glycidoxypropyltrimethoxysilane) sol-gel coating, Surf. Interface Anal. 50 (2018) 335–345, https://doi.org/10.1002/sia.6373.
[89] S.T. Abrahami, J.M.M. de Kok, V.C. Gudla, R. Ambat, H. Terryn, J.M.C. Mol, Interface strength and degradation of adhesively bonded porous aluminum oxides, Npj Mater. Degrad. (2017) 1, https://doi.org/10.1038/s41529-017-0007-0.
[90] R. Figueroa, X.R. Nóvoa, C. Pérez, Hydrophobic surface treatments for improving the corrosion resistance of anodized AA2024-T3 alloys, Electrochim. Acta 303 (2019) 56–66, https://doi.org/10.1016/j.electacta.2019.02.034.
[91] Ö. Özkanat, F.M. de Wit, J.H.W. De Wit, H. Terryn, J.M.C. Mol, Influence of pretreatments and aging on the adhesion performance of epoxy-coated aluminum, Surf. Coatings Technol. 215 (2013) 260–265, https://doi.org/10.1016/j.surfcoat.2012.07.096.
[92] A.A.C. Silva, T.I. Gomes, B.D.P. Martins, R.B.R. Garcia, L.D.S. Cividanes, E. Y. Kawachi, New insights in adhesive properties of hybrid epoxy-silane coatings for aluminum substrates: effect of composition and preparation methods, J. Inorg. Organomet. Polym. Mater. 30 (2020) 3105–3115, https://doi.org/10.1007/s10904-020-01468-y.
[93] P. Campestrini, E.P.M. Van Westing, H.W. Van Rooijen, J.H.W. De Wit, Relation between microstructural aspects of AA2024 and its corrosion behaviour investigated using AFM scanning potential technique, Corros. Sci. 42 (2000) 1853–1861.
[94] C.E. Moffitt, D.M. Wieliczka, H.K. Yasuda, An XPS study of the elemental enrichment on aluminum alloy surfaces from chemical cleaning, Surf. Coatings Technol. 137 (2001) 188–196, https://doi.org/10.1016/S0257-8972(00)01121-X.
[95] P.R. Underhill, A.N. Rider, Hydrated oxide film growth on aluminium alloys immersed in warm water, Surf. Coatings Technol. 192 (2005) 199–207, https://doi.org/10.1016/j.surfcoat.2004.10.011.
[96] J. Qu, Adhesion and fracture of polymer-metal interfaces. 7th Int Conf Therm Mech Multiphysics Simul Exp Micro-Electronics Micro-Systems, EuroSimE 2006 2006, 2006, https://doi.org/10.1109/ESIME.2006.1644063.
[97] N.W. Khun, G.S. Frankel, Effects of surface roughness, texture and polymer degradation on cathodic delamination of epoxy coated steel samples, Corros. Sci. 67 (2013) 152–160, https://doi.org/10.1016/j.corsci.2012.10.014.
[98] L. Novák, L. Fojtl, M. Kadlečková, L. Mañas, I. Smolková, L. Musilová, et al., Surface modification of metallic inserts for enhancing adhesion at the metal–polymer interface, Polymers (Basel) 13 (2021) 1–13, https://doi.org/10.3390/polym13224015.
[99] J.P.B. van Dam, S.T. Abrahami, A. Yilmaz, Y. Gonzalez-Garcia, H. Terryn, J.M. C. Mol, Effect of surface roughness and chemistry on the adhesion and durability of a steel-epoxy adhesive interface, Int. J. Adhes. Adhes. 96 (2020) 102450, https://doi.org/10.1016/j.ijadhadh.2019.102450.